NBSIR 80-2142 (Aluminum Association)

Plating on Aluminum

FILE COPY
DO NOT [...]

AUG 5 [...]

D. S. Lashmore

Corrosion and Electrodeposition Group
Chemical Stability and Corrosion Division
National Measurement Laboratory
U.S. Department of Commerce
National Bureau of Standards
Washington, DC 20234

November 1980

Final Report

PLATING ON ALUMINUM

D. S. Lashmore

Corrosion and Electrodeposition Group
Chemical Stability and Corrosion Division
National Measurement Laboratory
U.S. Department of Commerce
National Bureau of Standards
Washington, DC 20234

Table of Contents

1. Introduction:

This report covers the period from about July 1979 to February 1980 and includes, not only a discussion of work on both anodizing and immersion deposition, but also a summary of the results obtained over the last three years. A general theory of adhesion of metal coatings on metal substrates has been developed and adhesive energies were calculated for epitaxial zinc on aluminum. The case of a preexisting crack in the interface was considered.

The work on anodizing has resulted in a greatly improved understanding of adhesion mechanisms. The morphology of the initial stages of anodic film formation on aluminum alloy 7146-T6 has been characterized, yielding results rather different than predicted from commonly accepted theories. The morphology of nickel deposited into the pores of the anodic film has been characterized for the first time, it is believed, by <u>direct</u> TEM studies of cross sections of bulk specimens on which adhesion measurements have been made.

2. Program Summary:

The reader is urged to refer to particular progress reports
and to Plating 67, 37 (1980) and the Journal of the Electrochemical-
Society 127, 573 (1980) for more complete information on the first
two years' results. During the three years that the Aluminum
Association project Decorative Chrome Plating of Aluminum has been
carried out, three major areas have been worked on: immersion
deposition, anodizing, and the theory of adhesion between metal
coatings and substrates. A summary of the results follows:

2.1. Immersion Deposition:

2.1.1. Substrate Orientation:

It was shown in Progress Reports (P. R.) II-IV that the
substrate crystal structure plays an important role in both
the zincate and stannate processes. The dissolution of the
aluminum in the caustic zincate solutions is a sensitive
function of the crystallographic orientation. Moreover, zinc
was shown to form epitaxial deposits on all aluminum principal
planes. The bronze in the stannate process was shown to
exhibit a strong preferred orientation.

2.1.2. Cleaning Process:

In virtually every process for immersion deposition, a
caustic cleaning step is specified. The highly deformed
surface usually present on most material interferes with
epitaxial phenomena. In addition, this highly deformed layer
would be expected to dissolve more rapidly than less deformed
material, permitting a thick zinc deposit to form prefer-
entially at regions of high deformation. The etch cleaning
step not only removes the highly deformed material but also

attacks the same families of planes as the zincate and stannate electrolytes. This step is a necessity, if the balance between aluminum dissolution and uniform zinc deposition is to be maintained.

2.1.3. <u>Alloy Constituents</u>:

It was shown that even small traces of magnesium determine the sites at which large zinc crystallites grow. The epitaxial phenomena observed on pure aluminum were also observed on one alloy (6061-T6) and probably exist on others (P. R. II & III). Investigations of adhesion correlations with alloying constituent were discussed in P. R. IV. Pure aluminum exhibited greater adhesion than did the alloys investigated here.

2.1.4. <u>Effect of Ferric Chloride and Rochelle Salts</u>:

It was shown that small additions of ferric chloride and Rochelle salts have a major effect on the deposition process. When absent, it was shown that three atoms of zinc are deposited for every two atoms of aluminum dissolved. When present, it was shown that almost nine atoms of aluminum are dissolved for each atom of zinc deposited. (See P. R. II.) It was shown that iron is deposited (by immersion or perhaps chemisorption) before the bulk of the zinc. Following a nitric acid immersion (the double zincate procedure), it was shown by Rutherford back scattering experiments (P. R. III) that about two monolayers of iron and two monolayers of zinc were left on the surface. Transmission electron microscopy of double zincated specimens indicated the existence of an iron zinc alloy formed just at the aluminum surface. (See P. R. I-IV.)

2.1.5. <u>Morphology</u>:

The morphology of immersion deposits was characterized by optical, SEM and TEM techniques, both on pure aluminum and on a number of alloys. See P. R. I-IV, Plating <u>67</u>, 37 (1980), and J. Electrochem. Soc. <u>127</u>, 573 (1980). Zinc forms epitaxial deposits on the aluminum substrates so that Zn:

(0001) < 10$\bar{1}$0 > //Al (100) < 010 >, Zn:

(0001) < 11$\bar{2}$0 > //Al (111) < 1$\bar{1}$0 > and Zn:

(0001) < 11$\bar{2}$0 > //Al (1$\bar{1}$0) < 11$\bar{1}$ >.

2.1.6. <u>The Stannate Process</u>:

It was shown by TEM that tin crystallites cover the surface following the stannate immersion process. The tin was shown to deposit in three distinct morphologies (See P. R. II.): (1) the formation of a fine grained deposit (<20Å) completely covering the surface; (2) at a later time, the formation of small crystallites in discrete areas; and, finally, (3) the growth of large, almost spherical clusters. It seems that stage III is just barely reached after about 45 seconds in the electrolyte.

The bronze layer deposited as part of the stannate process was shown to exhibit a strong preferred orientation. However, extensive work on this phenomenon was not done because of the proprietary nature, of the commercial process of which it is a part.

Significantly, it was shown that there are important adhesion variations from the top to the bottom of vertically

plated specimens. The greatest adhesion occurred on the lower part. Apparently, this phenomenon was also revealed in the field by corrosion variations on plated bumpers.

Adhesion on a number of alloys was characterized by peel testing. Deposition on single crystal spheres indicated that a similar deposition mechanism existed with the zincate process, (P. R. II, III & IV).

2.1.7. Field Ion Microscopy (F.I.M.)

Techniques were developed to image zinc coated aluminum in the F.I.M. (see P. R. IV). The zinc was observed to form blade shaped deposits on the aluminum tips, probably due to selective deposition on certain crystallographic planes.

2.1.9. Scanning Voltammetry and Acid Dissolution Data:

Scanning voltammetric data indicated that the deposition of an iron-zinc or iron layer precedes the deposition of the zinc. By monitoring the substrate potential as a function of time, a modified procedure for depositing a thin layer of zinc or zinc-iron alloy was developed (see Interim Report, Aug. 1979, and section 4.2 of this report).

2.2. Anodizing Pretreatments

2.2.1. Effect of Structure

A procedure was developed to enable direct TEM micrographs of cross sections of anodized aluminum coated with nickel. Apparently, this is the first time that specimens of this type have been prepared, though it should be noted that there has been much published on replicas of anodic films and on

microtomed anodized aluminum. The data shown in this report reveals <u>no</u> penetration of the barrier layer by the nickel, ruling out metallic bonding as an adhesion mechanism.

The initial states of pore formation were characterized by direct TEM studies of anodized 7021-T63 and 7146-T6. The initial stages of growth were shown to be much different from subsequent stages. The anodic oxide seemed to form small square regions which grew together like building blocks on a (100) aluminum substrate (see section <u>3.2.2</u> of this report). This evidence indicates the important role played by the structure of the substrate during the initial stages of growth. The classical model of pore growth requires a field assisted dissolution of the aluminum at places where the oxide is thinnest, and such a model is supported by the results obtained during this study. However, in the initial stages of oxide formation the thin areas are <u>not</u> necessarily associated with pore formation; indeed, it was shown that oxide growth can be quite remote from the dissolution sites, as can the initial pore structures.

2.2.2. <u>Effect of Anodizing Parameters on Adhesion</u>:

It was shown that adhesion is an approximately linear function of the applied voltage. Since the cell diameter also increases in a linear manner with the applied voltage, a relationship was thought to exist between adhesion and pore diameter. Moreover, the greater the cell diameter, the less oxide there is per unit area of the coating. This implies that the strength of the oxide itself is the determining

factor (or weak link) in adhesion of subsequent coatings to the anodic film. It should be noted that the pore structure, especially at higher voltages, does not vary much as one changes from one of the three major electrolytes used for this process (sulfuric acid, oxalic acid, and phosphoric acid) to another even though adhesion of subsequent coatings can vary by more than an order of magnitude between the various electrolytes. Therefore, the adhesion does not appear to be dependent upon the pore structure, but, rather, upon the nature of the oxide itself. The composition of the anodic film, varies considerably with the alloy and with the electrolyte.

It was shown (see section 3.1 of this report) that the the use of an 0.5 percent solution of HF in place of sulfuric acid on 7146-T6, results in increased adhesion.

2.3. Theory of Adhesion for Metallic Coatings on Metallic Substrates:

2.3.1. A theory of the adhesive energy for metallic:

coatings on metallic substrates was discussed om detail (see section 5 of this report). The theory takes into account the effect of structure through a parameter 'a' which represents the lattice parameter in the interface. This parameter is determined by the orientation of both the substrate crystal and the coating crystal. The adhesive energy as a function only of the structure is

$$E_{ad} = \frac{K\,G_o\,a^2}{(2\pi)^2 d}\,.$$ [1]

For f.c.c. materials, $K = 3$, G_o is the shear modulus in the interface which can be determined from the binding energy between the two metals and d is the distance of closest approach. The lattice parameter in the interface, a, is given by:

$$a = \frac{2a_c a_s}{a_c + a_s} .$$ [2]

2.3.2. In many cases perfect epitaxy is not possible; therefore, the misfit between the coating and the substrate has to be taken into account. It was shown (see section 5.1 of this report), that the adhesive energy in the case of significant misfit is given by:

$$E_{ad} = \frac{KG_o a^2}{(2\pi)^2 d} - E_d - E_s$$ [3]

where E_d is the dislocation energy per unit area and E_s is the distributed strain energy per unit area. A special case was calculated for zinc coatings on aluminum whose epitaxial relationships were characterized during this program.

2.3.4. The case of a preexisting crack of length 2 c, in the interface was considered, and a Griffith type equation for the minimum stress, σcritical, necessary to propagate this crack (and thus to cause adhesive failure) was derived as:

$$\sigma\text{critical} = \sqrt{\frac{2(\gamma_c + \gamma_s)}{\pi c \left(\frac{1}{E_c} + \frac{1}{E_s}\right)}} .$$ [4]

This equation will be improved in the future to include
the effect of strain energy which may be in many cases an
important term.

III. Phosphoric Acid Anodizing Prior to Plating:

3.1. Adhesion Data:

A number of experiments concerned with anodizing of aluminum alloys were performed. A great deal of data has been made available by Wittrock, so the experiments described here were designed to compliment the available literature. The experiments were specifically set up: (a) to characterize the effect on adhesion of variations in the applied anodizing voltage. Surprisingly, no direct data on this subject seems to be available, (b) to examine the effect of post-anodizing treatment on adhesion, and (c) to extend Wittrock's measurements of adhesion as a function of anodizing electrolyte temperature.

3.1.1. Adhesion versus anodizing voltage:

The alloy chosen for this study was 7146-T6 because it is in wide use as a bumper alloy. Studies on 7129-T63 will be reported in the future. Specimens of 5 cm x 10 cm x 0.64 cm were buffed, and degreased with trichloroethleyne in an ultrsonic cleaner. Following this treatment, the specimens were further polished with 0.01 μm MgO by hand, given a 30 second treatment in 50 percent nitric acid in an ultrasonic cleaner, rinsed in distilled water, and immediately anodized. The total anodizing charge (for adhesion test specimens) was standardized to about 20 coulombs/cm^2 regardless of anodizing time. An amp-hour meter was used to monitor the total charge. Following the anodization process, the specimens were given a

post treatment, typically in an electrolyte of 2 g/L sulfamic
acid held at 55-60 °C. The specimens were then rinsed in
distilled water and placed in a nickel sulfamate electrolyte,
maintained at a pH of 2.5 for 60 seconds prior to applying a
potential. This potential was increased at a very slow rate
in such a way that the current density went from 0 to 4.3
amps/dm^2 in about 5 minutes. Adhesion was measured by peel
testing. All specimens were plated with a 150 μm thickness of
nickel.

The adhesion was found to be an approximate <u>linear</u> function
of anodizing voltage (figure 1). The extended curves intercept
the x-axis at about 15 volts, indicating that 15 V is the
threshold below which the adhesion is zero. The slope of the
curve, however, changed with the concentration of the acid.
The current density versus applied voltage has been superimposed
on this data, showing that the greatest adhesion occurs when
the current density is about to become unstable. The electrolyte
was agitated mechanically. Because the limiting current
density is dependent on agitation, the curves shown in figure 1
may not represent the maximum obtainable current density, even
though the mixing was quite virorous.

The linear <u>increase</u> of adhesion with anodizing voltage is
unexpected if the major bonding forces are Van Der Waals, as
thought by Alexsandrov (1), or even if they are due to ionic
or covalent bonding. The cell diameter as a function of
applied voltage, figure 2 as calculated from the data of
Keller, Hunter and Robinson (2). It should be noted that

Figure caption for figure 1 (page 13).

Figure 1. Adhesion and current density as a function of anodizing voltage (a) 10 percent phosphoric acid, 60 °C, (b) three percent phosphoric acid, 60 °C, and (c) 10 percent phosphoric acid, 30 °C.
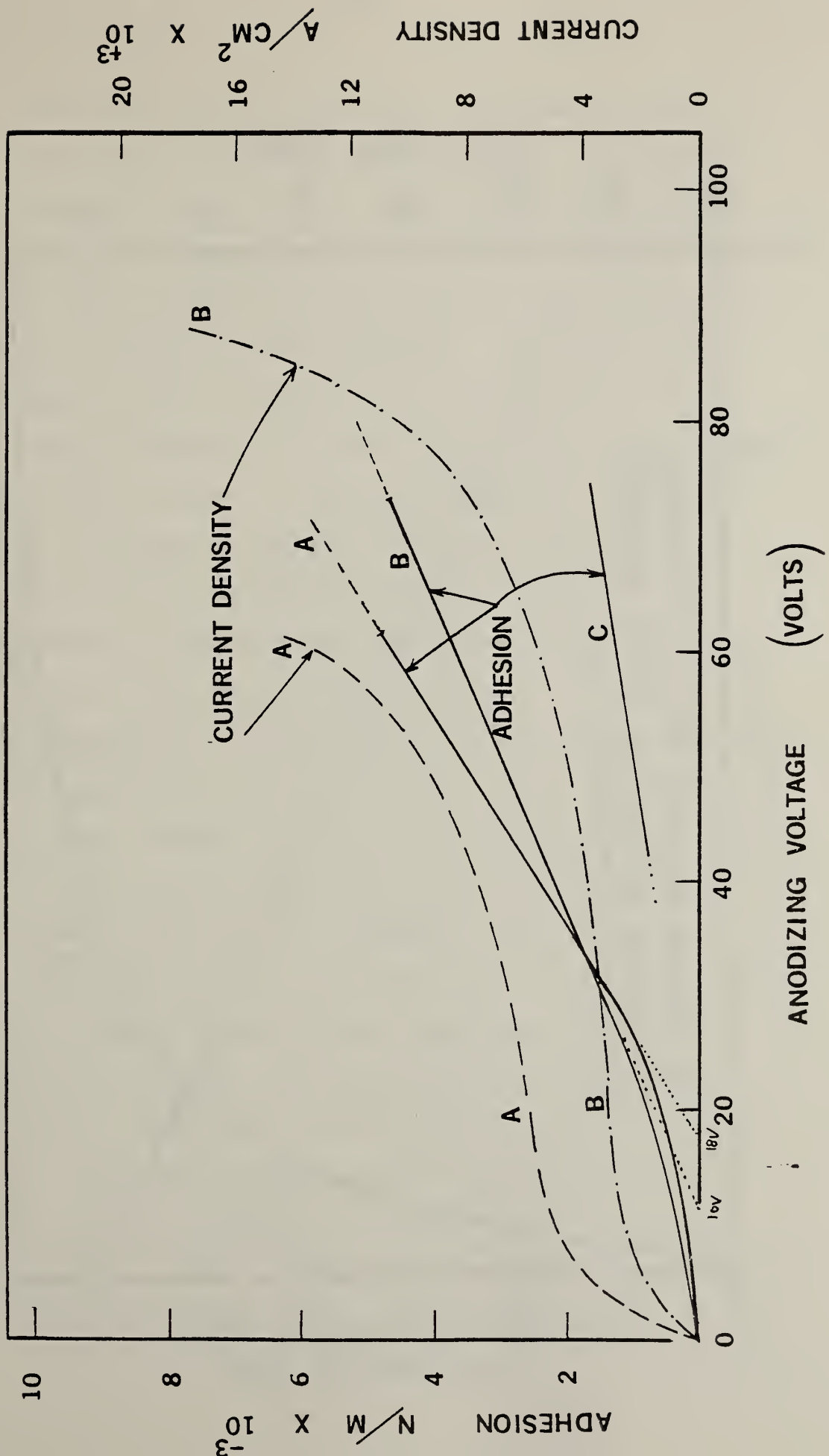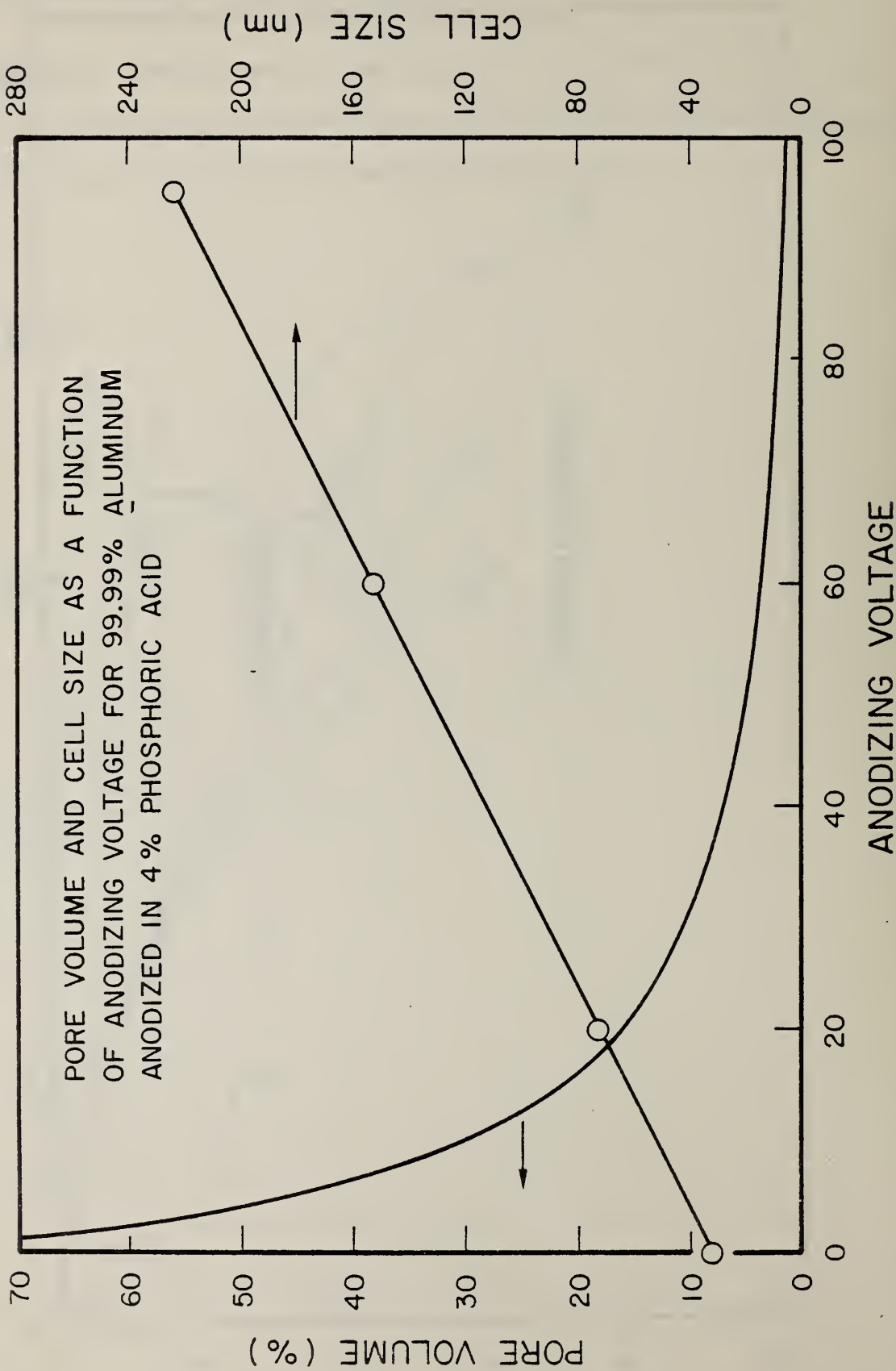
Fig. 1.

Figure 2. Pore volume and cell size as a function of anodizing voltage for 99.99% aluminum anodized in 4% phosphoric acid.

O'Sullivan and Wood (3) have shown that the pore diameter is
also linearily dependent on applied voltage. If the bonding
between the pore walls were solely responsible for adhesion,
then, as the area available for bonding increased with decreasing
voltage, the adhesion would also be expected to increase. The
data in figure 2, compared to figure 1, show exactly the
opposite trend. As the area for bonding increases, the
adhesion decreases. The adhesion as a function of pore diameter
is shown in figure 3. The linear dependence of adhesion on
cell size shown in figure 2, implies that the oxide is the
weak link. As the proportion of oxide in the anodic film
decreases at higher voltages, the adhesion increases. This
finding is consistent with other evidence. For example, the
microstructure of the anodic film as shown by many investigators
is essentially the same on all alloys, even on pure aluminum.
At higher voltages, as shown by Keller, Hunter and Robinson,
the pore microstructure does not vary much between different
anodizing electrolytes. For example, oxalic acid, sulfuric
acid and phosphoric acid all give rise to similar pore diameters
at voltages of around 60 volts, though adhesion variations
between alloys and even electrolytes can be more than three
orders of magnitude. This new evidence indicates that efforts
to improve adhesion of the anodic film should be directed at
increasing the strength of the oxide itself. It should be
noted that metallic bonding through the base of the pore by
the nickel has been ruled out by the TEM evidence.

ADHESION AS A FUNCTION OF CELL SIZE

7146 T6

CELL SIZE nm
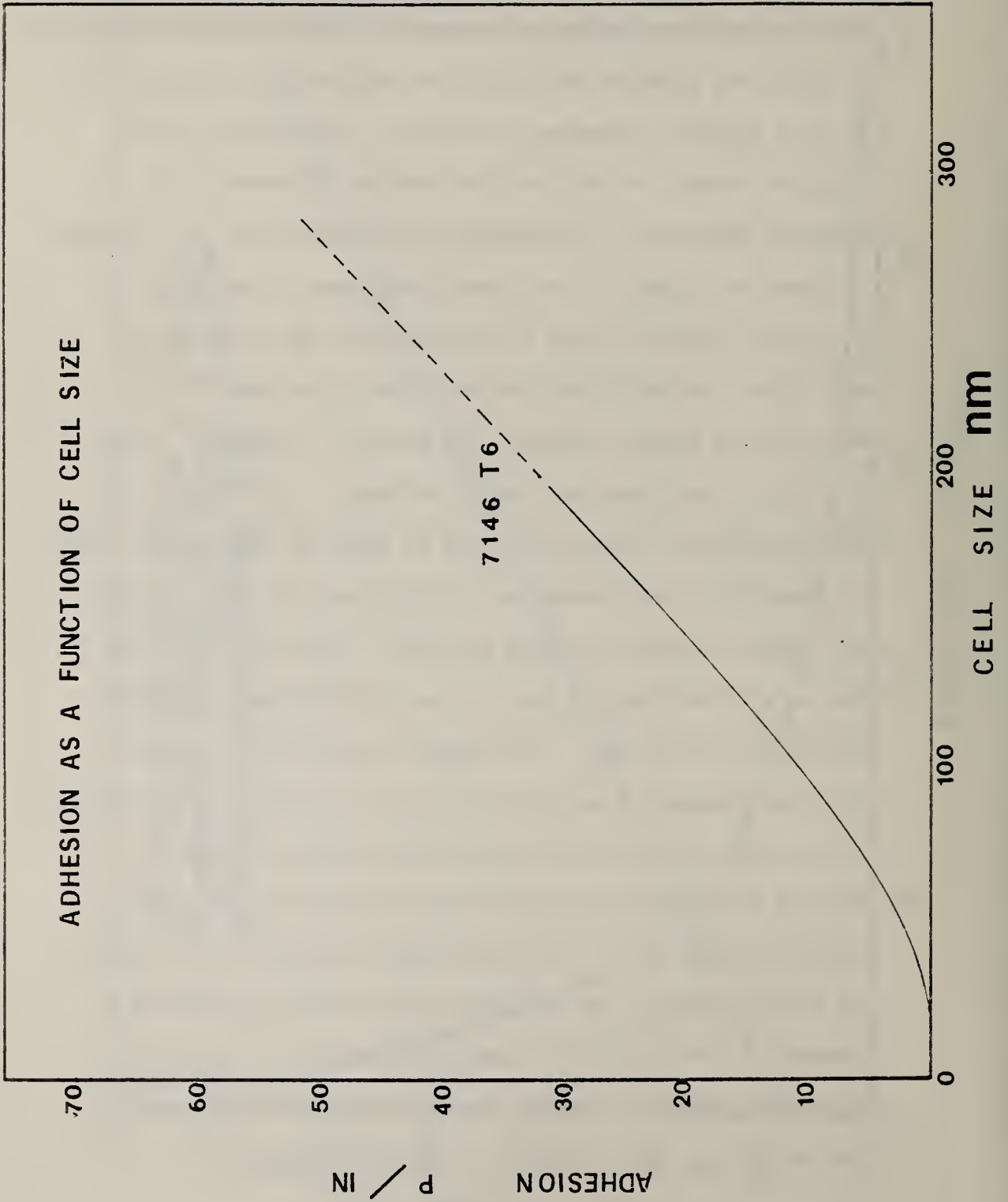
ADHESION P / IN

3.1.2. The Effect of Post Anodizing Treatment:

Extensive experiments on post anodizing treatments have not yet been done. However, preliminary experiments indicate that dilute HF (0.5 vol. percent) solutions provide greater adhesion than the commonly used sulfamic acid. However if more concentrated solutions are used, say 2 g/L, then the adhesion drops off. If the concentration of the sulfamic acid is increased to 4 g/L, then adhesion increases by about 25 percent. The strong HF solutions obviously attacks the oxide, more rapidly than the sulfamic acid.

A possible explanation for the effect of the post anodizing treatment is that the acid removes a weak boundary layer from the pore walls and further cleans out those pores filled with reaction products.

3.2. Microstructure of the Anodic Film:

In order to determine the mechanism of adhesion of nickel, plated in a porous anodic film, a transmission electron microscopy (TEM) investigation of the microstructure was undertaken. Specimens of several different kinds of alloys were investigated and were prepared in either of two ways,: (a) so that the interface was perpendicular to the electron beam, or (b) so that the interface was parallel to the beam. Data from case (b) have not been reported in the literature. Therefore, this investigation represents, the first time that a direct TEM study of nickel plated into the anodic film has been characterized by TEM. The few TEM studies of anodized specimens (not nickel plated) prepared with the interface parallel to the beam were

either of replicas or were of specimens prepared by ultra-microtome techniques.

Anodic film on both 7129-T63 and 7146-T6 were investigated. The specimens were anodized according to Wittrock's procedure. The starting geometry was 10 cm x 10 cm x 0.64 cm (4" x 4" x 1/4") for 7146-T6 and about 5 cm x 15 cm x 0.64 cm (2" x 6" x 1/4") for 7129-T63. The large specimens were used for adhesion determination prior to further preparation. It was thought important to know how an interfacial structure under study was related to a given adhesion value. Following adhesion testing, an untested section near the center of the panel was nickel plated for an extended time in the same sulfamite nickel electrolyte used for peel testing. The plating was continued until 5 mm of nickel was built up.

Foils were then prepared from this specimen so that the interface was perpendicular to the surface — the interface would appear as a line through the foil. Two techniques were used to cut foils: (a) a spark cutter, and (b) a LECO - VARI CUT (VC-50) low speed diamond cut off saw. Foil thickness varied from 75 to 250 μm. The foils prepared by spark cutting were further polished using standard metallographic techniques, with the final polish being 0.01 μm MgO. The diamond cut-off specimens were used without further processing. Both sets of foils were then thinned to electron transparency in an ion - milling machine with 3.5 to 4 KeV Argon ions. This latter technique required milling times in excess of a week, operating 24 hours/day. The thinned foils were then examined in a

Phillips EM 200 A at 100 keV, equipped with the usual anti-contamination stage and a double tilt specimen holder.

3.2.1. A representative micrograph of 7129-T63 anodized in 3 percent phosphoric acid is shown in figure 4. The adhesion, measured by peel testing, exceeded 75 N/m (100 #/in.) The average cell size, <u>at the interface</u>, is about 1250 $\overset{\circ}{A}$, yielding a cell density of 6.4 x $10^9/cm^2$. The tip radius is about 850 $\overset{\circ}{A}$. Several important structural features of the anodic oxide - nickel system are revealed here. First, the nickel has penetrated the pores completely and, secondly, there appears to be a continuous oxide barrier between the nickel and the aluminum. The nickel grain size in this specimen is about 400 - 500 $\overset{\circ}{A}$. For this micrograph, the substrate was not oriented for dislocation contrast, so the effect of the aluminum's structure on the growth of the anodic film was not apparent.

The aluminum's structure has a very important effect on the growth of the anodic film, as shown in figure 5.   This micrograph was exposed and printed to bring out the dislocation structure. It is seen that, in a number of places, the oxide grows along dislocations. Regions of oxides of 150 $\overset{\circ}{A}$ diameter appear to precede the aluminum/oxide interface by as much as 1200 $\overset{\circ}{A}$. Moreover, many of the oxide regions appear to have four fold symmetry (though no diffraction from them was observed).

As the ion thinning proceeded into the nickel, it became apparent that the pores (filled with nickel) were not at all uniform, but underwent a great deal of branching, as shown in figure 6 abc. This branching is probably caused by a voltage
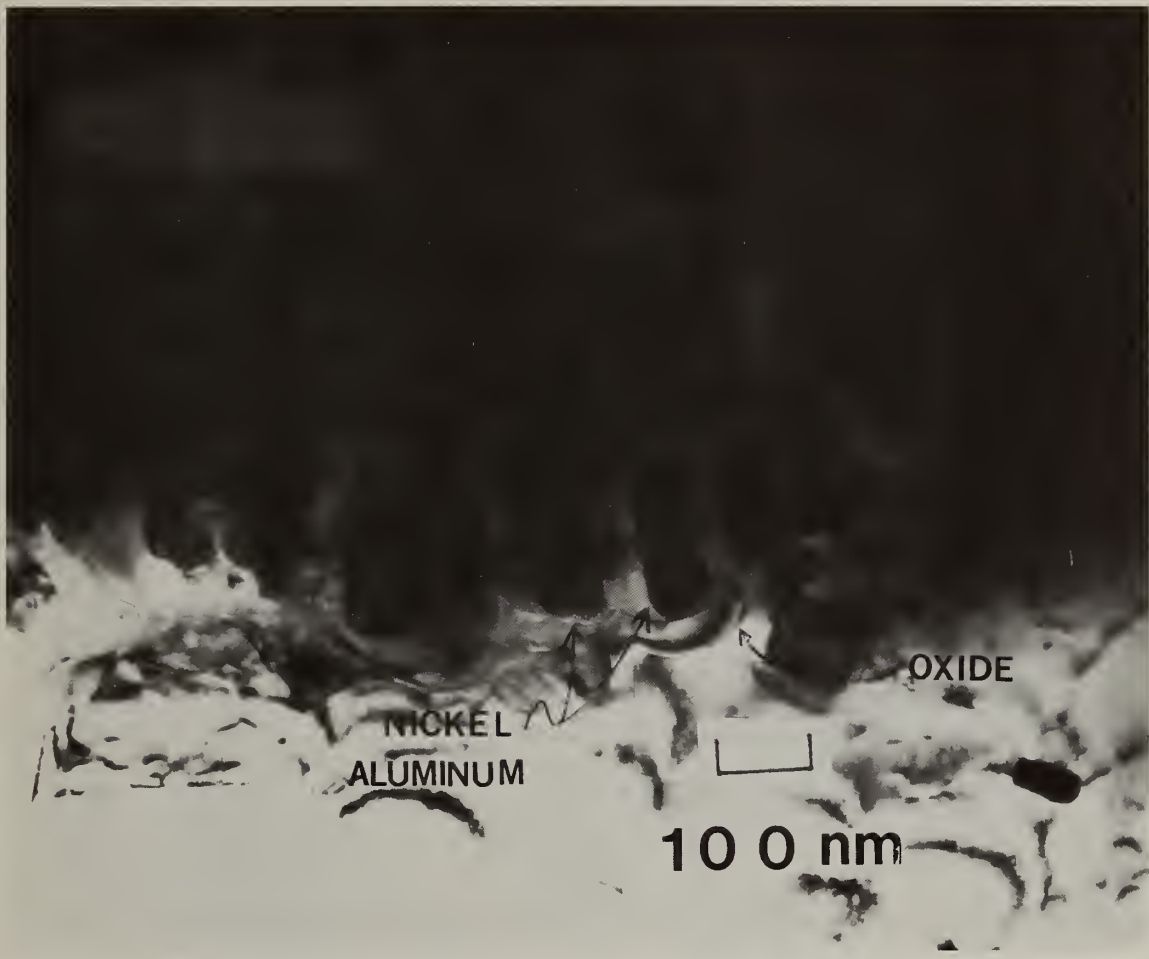
Figure 4. A transmission electron micrograph of 7129 T63 anodized in 3% phosphoric acid then plated with nickel from a sulfamate electrolyte.
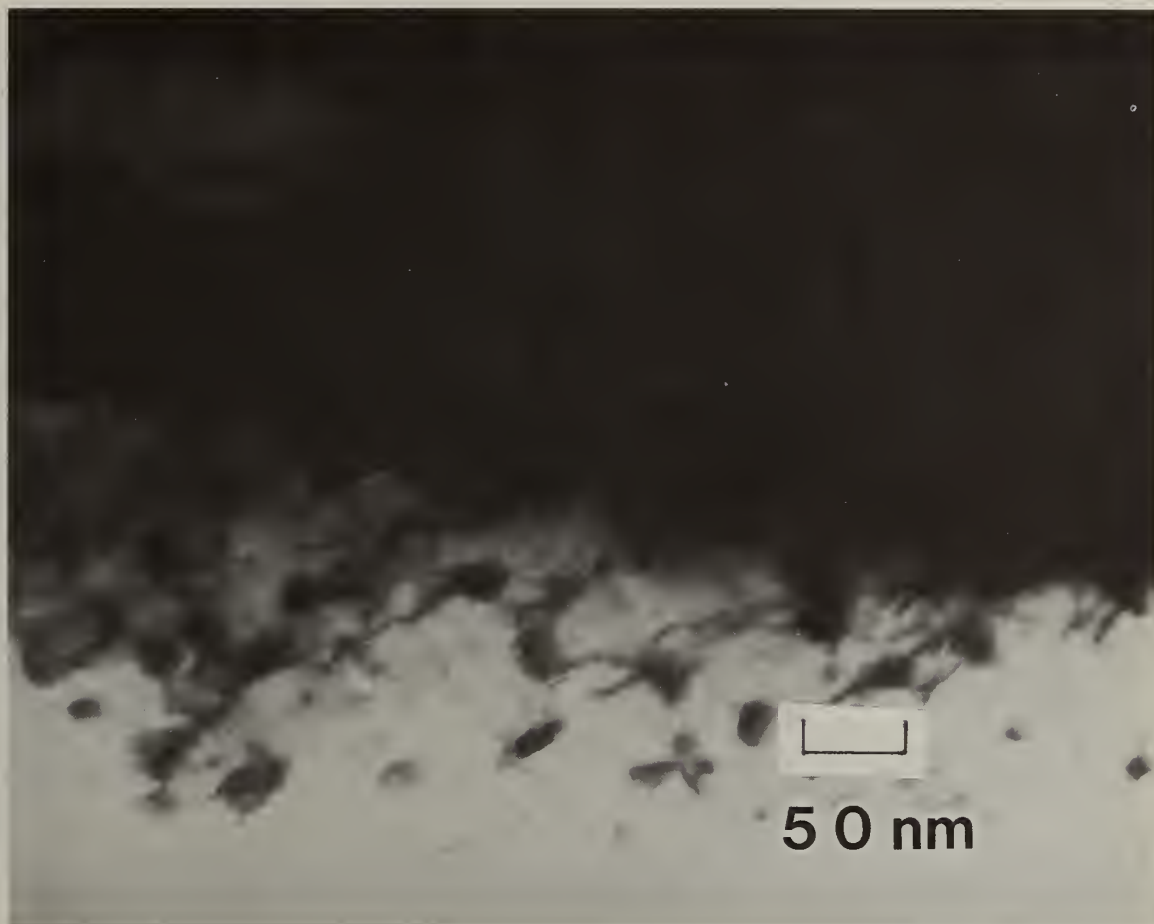
-21-

Figure 5. A TEM micrograph of 7129 T63 showing the growth of the anodic
oxide along dislocations in advance of the barrier layer. The dark area
coeresponds to nickel plated into the porous oxide.
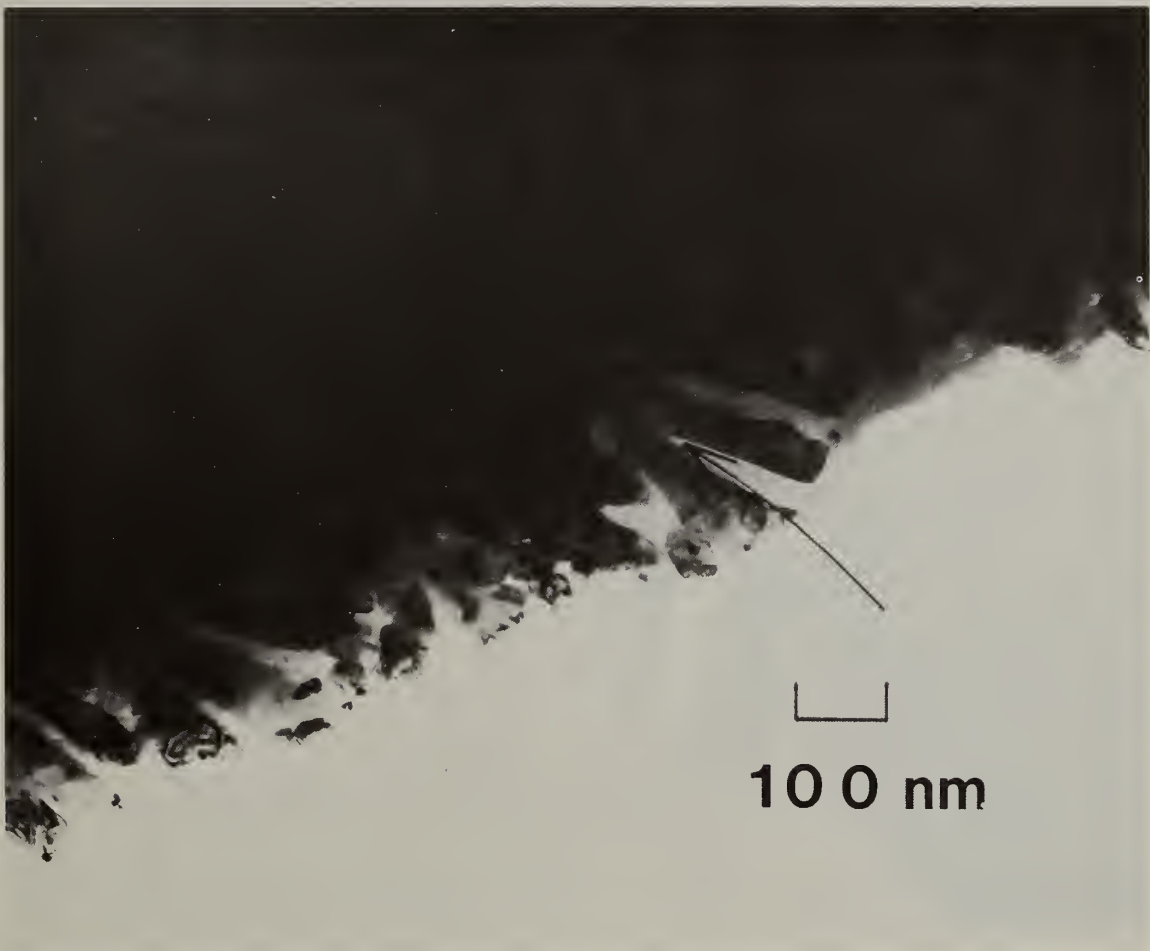
Figure 6a. A low magnification bright field TEM micrograph of nickel
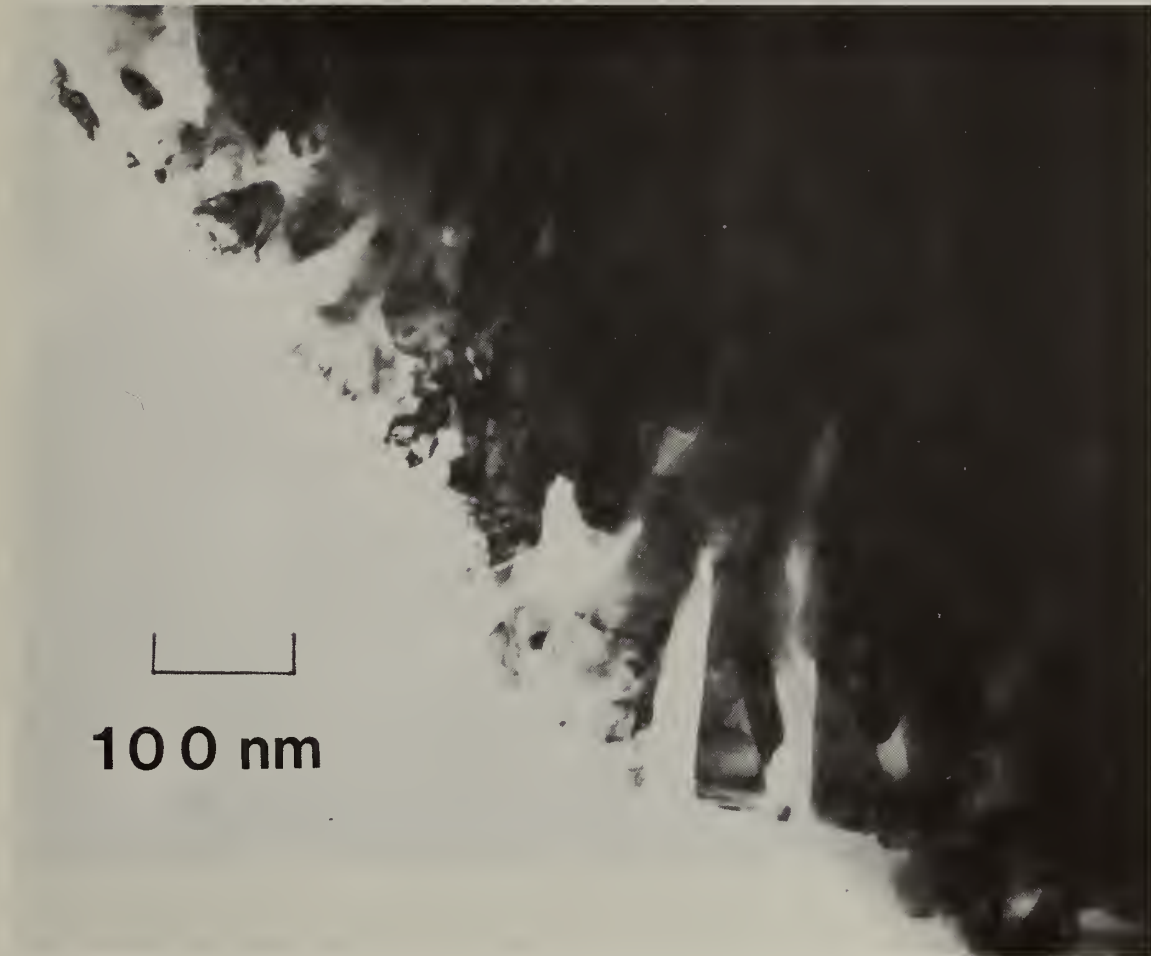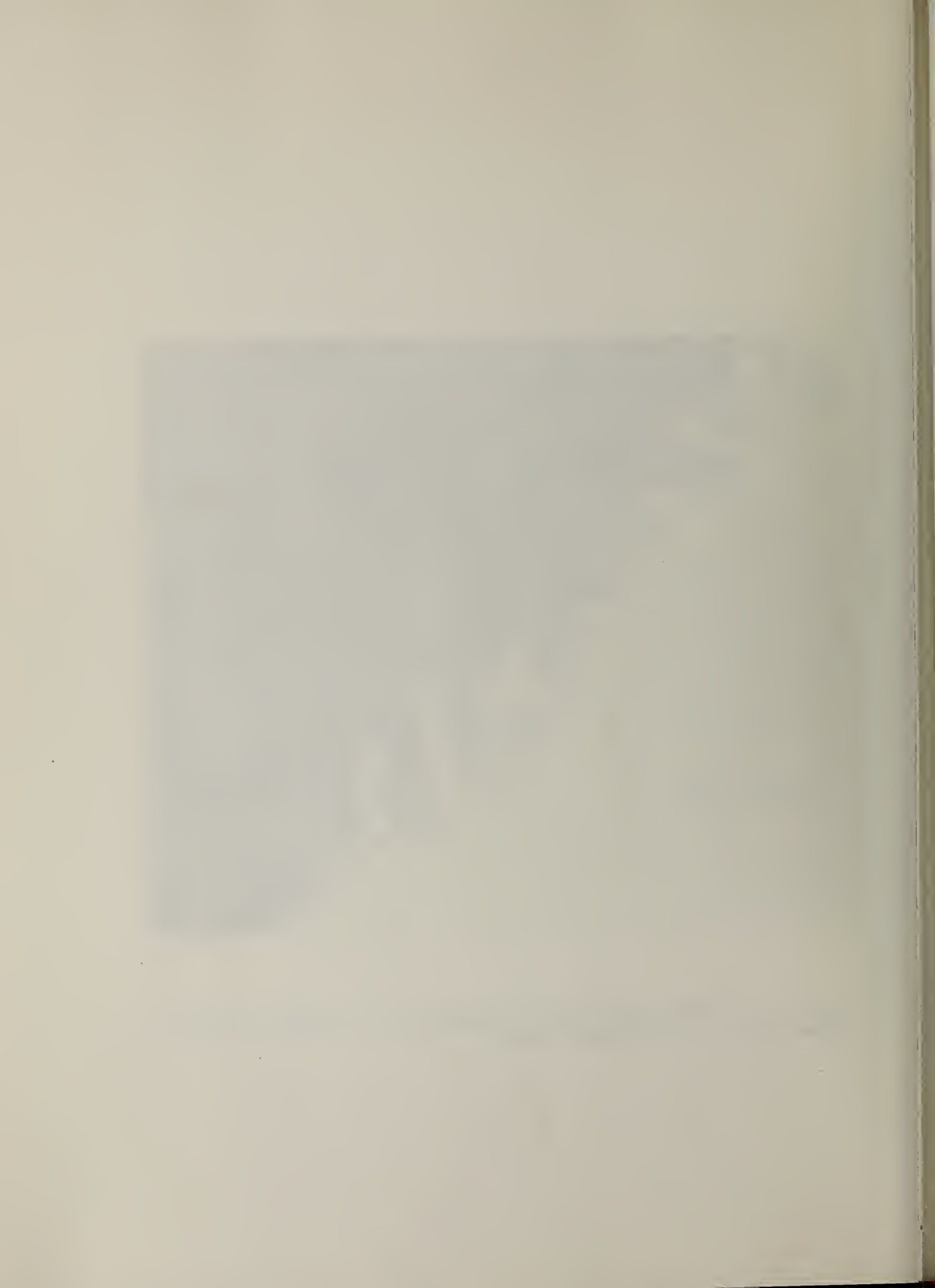plated into a porous anodic oxide exhibiting typical pore branching.

100 nm

Figure 6b. A TEM bright field micrograph of the same srea as shown in figure 6a but at higher magnification.
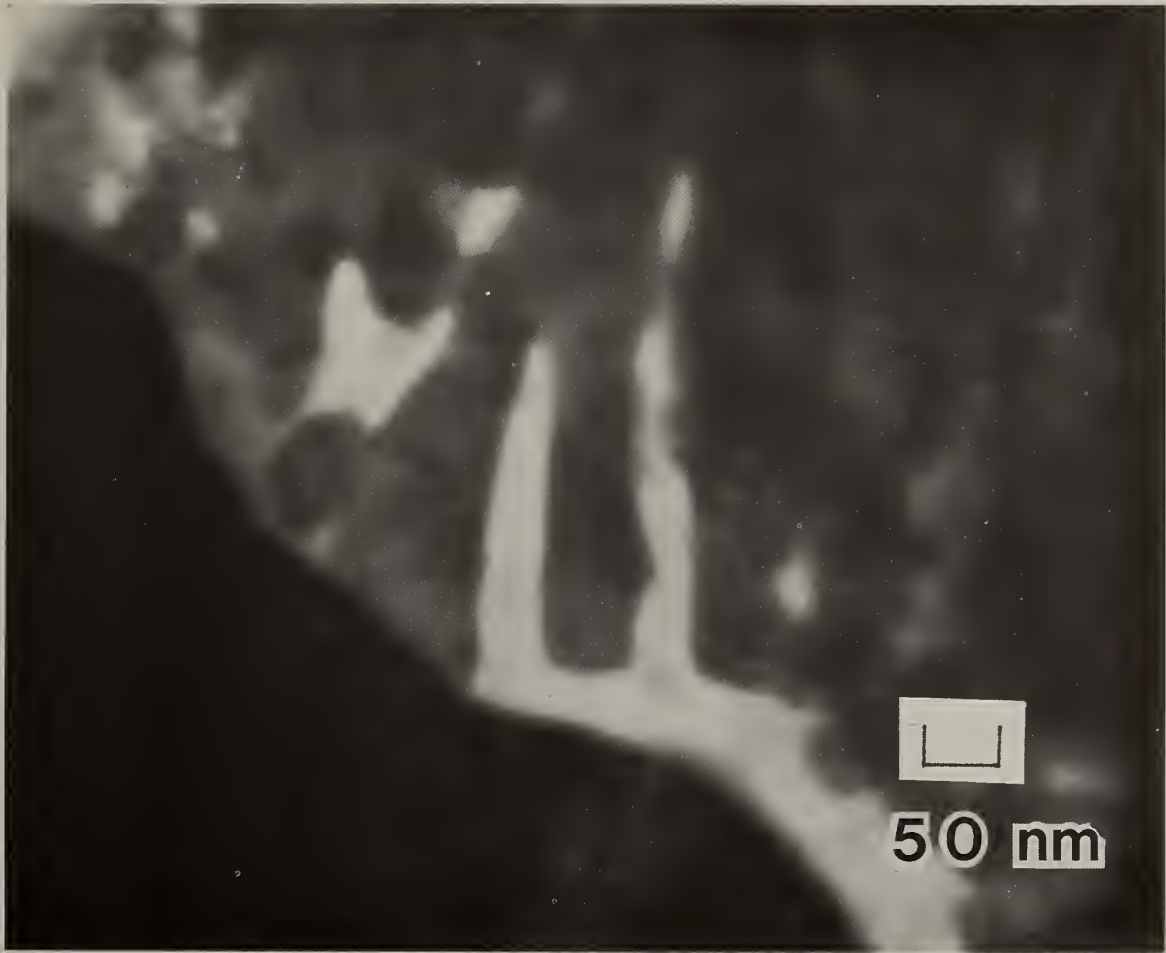
Figure 6c. A Dark field micrograph of the same area as shown in 6a taken with the objective aperature over the diffuse oxide ring.

transient at the initial stages of film growth. Certainly
this type of microstructure would result in a strong mechanical
bonding.

3.2.2. The initial stages of growth of the anodic film on specimens
of 7146-T6 were studied by TEM, with the beam perpendicular to
the interface. The mechanism of initial film formation is
apparently different from growth at a latter stage. Several
surprising results were observed in figure 7. A large number
of rectangular and even square regions of oxide are observed
on the (100) plane of 7146-T6. This observation indicates
that a strong role is played by the structure of the substrate.
These regions of oxide grow in such a way as to form pores, as
indicated on the micrograph. Even the large pores show evidence
of being made up of rectangular 'building blocks' of oxide.
The second major feature observed during the initial stage of
film formation is a large number of fringes which may be Moiré
fringes. If subsequent study shows this to be the case, then
it is clear that the oxide forms, at least at the initial
stage, an epitaxial (or perhaps pseudomorphic) layer before
becoming amorphous. No evidence of crystalline oxide was
detected in the diffraction patterns.

The white areas shown in figure 7 are etch pits. The
classical model of pore growth requires field assisted dissolution
at places where the oxide is weakest and this model is supported
by the evidence in Figure 4. However, in the initial stages
of oxide formation, the weak areas are not necessarily associated

Figure 7. A TEM micrograph of the initial stages of anodic film formation on
7146 T6.   The electron beam is now perpindicular to the interface.
Note that the surface is covered with Moire fringes which may indicate an
epitaxial oxide forms during the initial stages of anodization.

with pores or even regions of oxide thickening. Indeed, the
oxide growth is remote from the dissolution sites. Some pores
contain only a few dissolution sites and some none at all.
Thus, initially the film formation mechanism can be quite
different from latter stages. Further evidence for this is
shown in figure 8, where aluminum dissolution is observed to
occur on the outside of a large pore. In this figure, a
number of well developed pores are also observed to have no
evidence of dissolution at their base; just the opposite, the
base of the pores seems to be filling in with oxide. It is
thought, however, that once the surface is covered uniformly
with oxide, the oxide will redissolve within the pore base.
Very large crystallographic regions of oxide are apparent in
this micrograph.

At a latter stage of growth, as shown in figure 9, the
pores take a more classical appearance. However, note that
both the inside and outside of the pore walls have a structure
distinct from the interior material. It is thought that the
interior material is removed during the post anodizing treatment.

The microstructure of the equilibrium oxide structure
oxide is presented in figure 10. The small pore diameter
present at the initial stage of growth gives way to a pore
diameter characteristic of the applied potential and dissolution
now takes place through the base of the pore. This is shown
in this dark field micrograph as a black area in the pore
center. The observations made above are shown schematically
in figure 11.
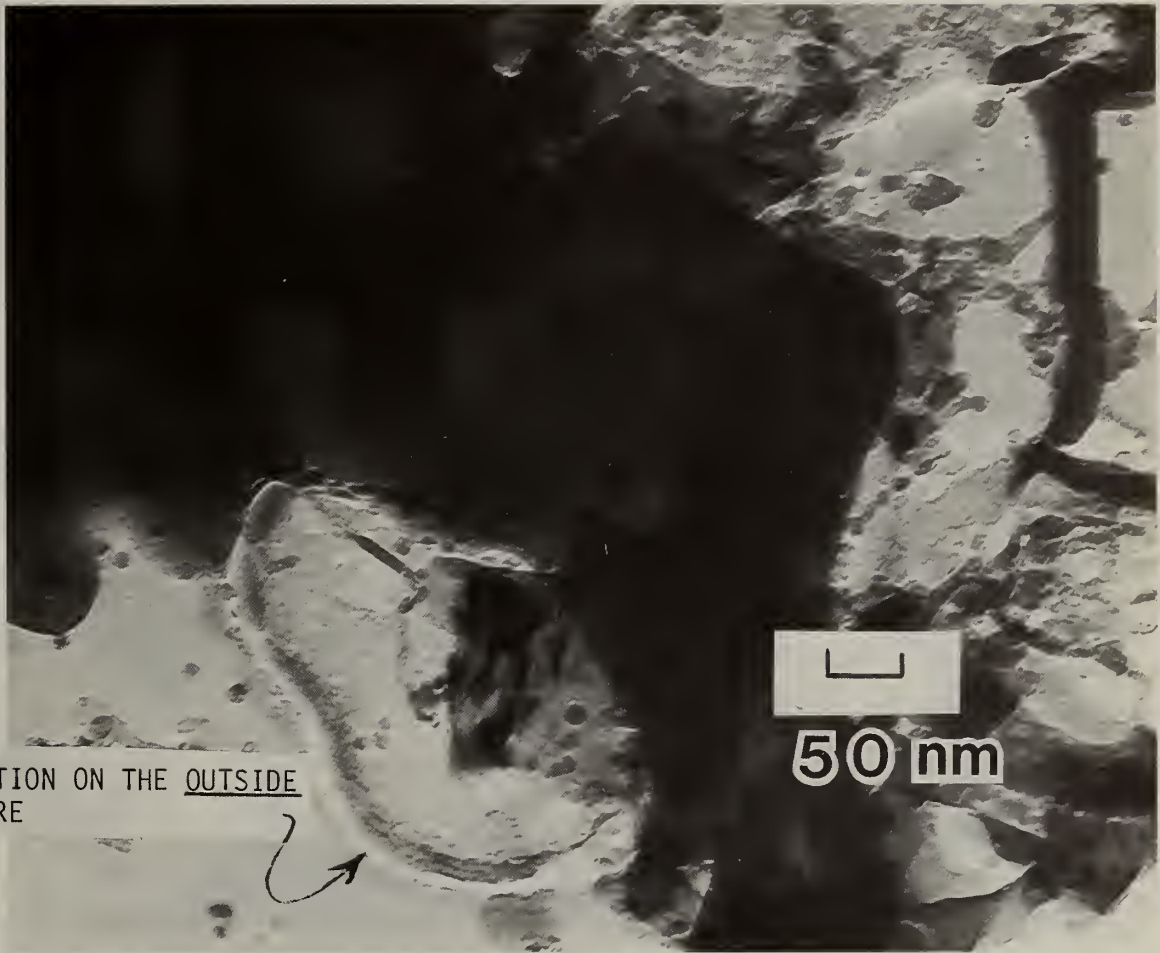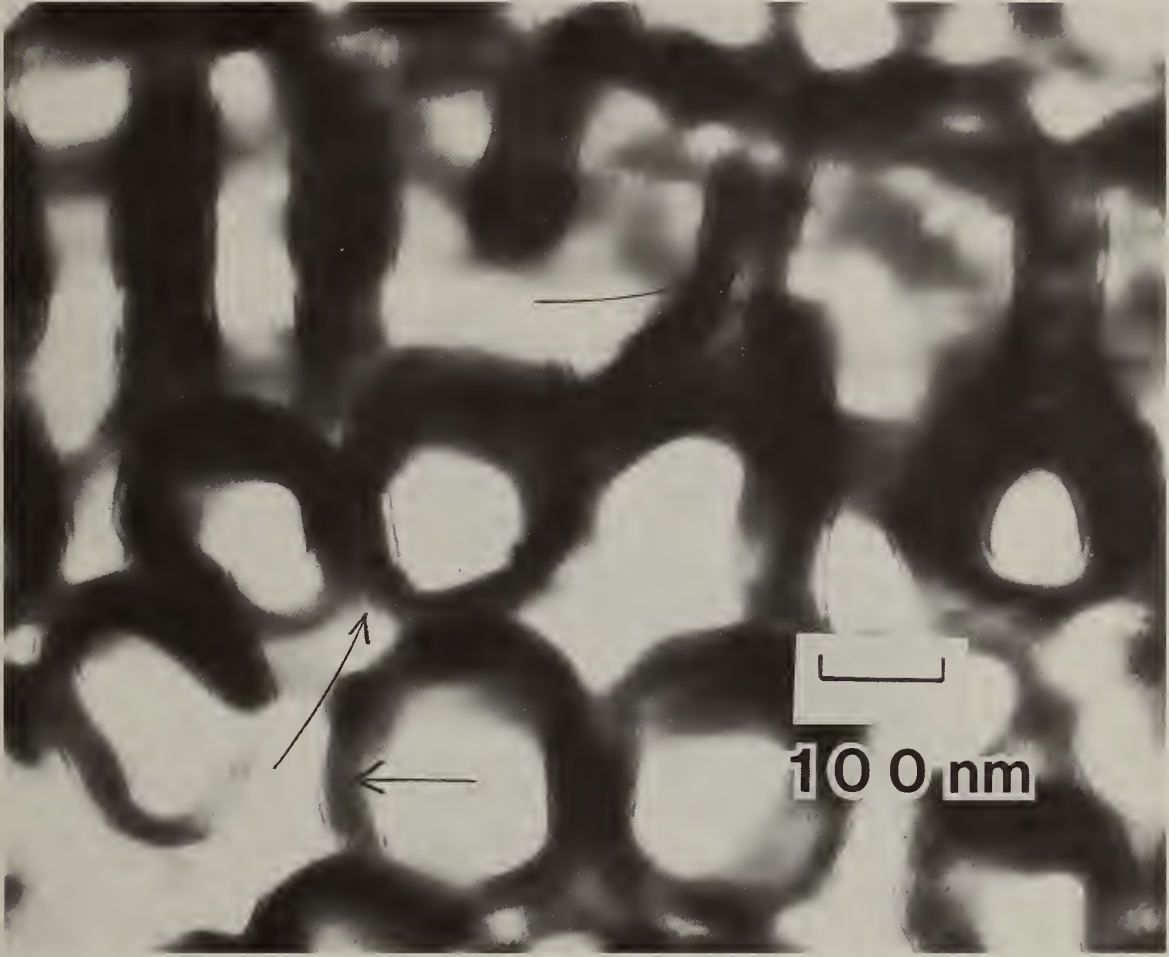
DISSOLUTION ON THE <u>OUTSIDE</u>
OF A PORE

50 nm
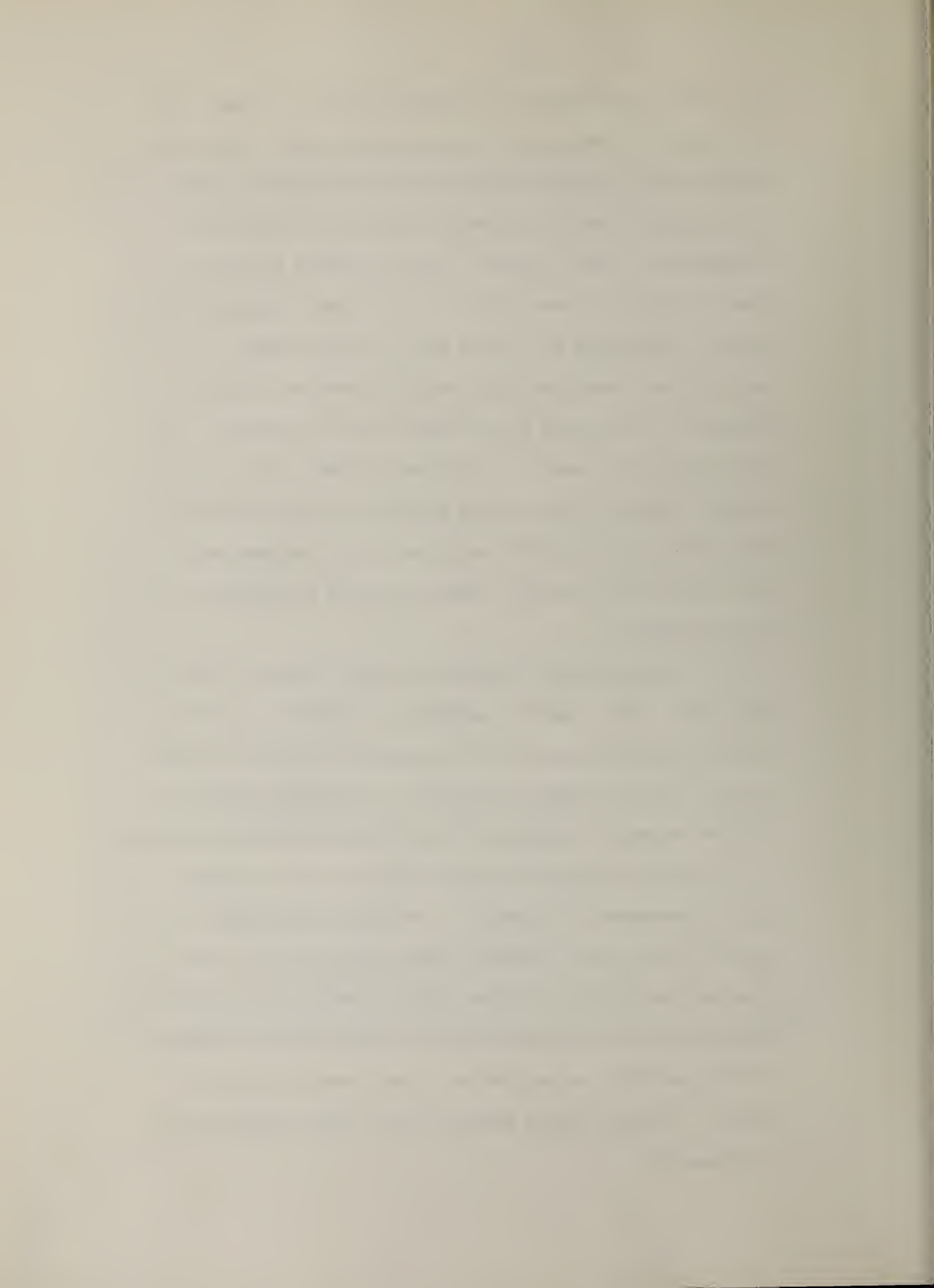
Figure 8. A TEM micrograph showing dissolution of the aluminum around the
outside of an established pre rather than through its center as in the
classica model of Keller, Hunter and Robinson. Note that this behavior
is only observed during the intiial stages of growth.

Figure 9. A TEM micrograph of a latter stage of film formation on 7129 T63 indicating the existance of a substructure to the cell walls.
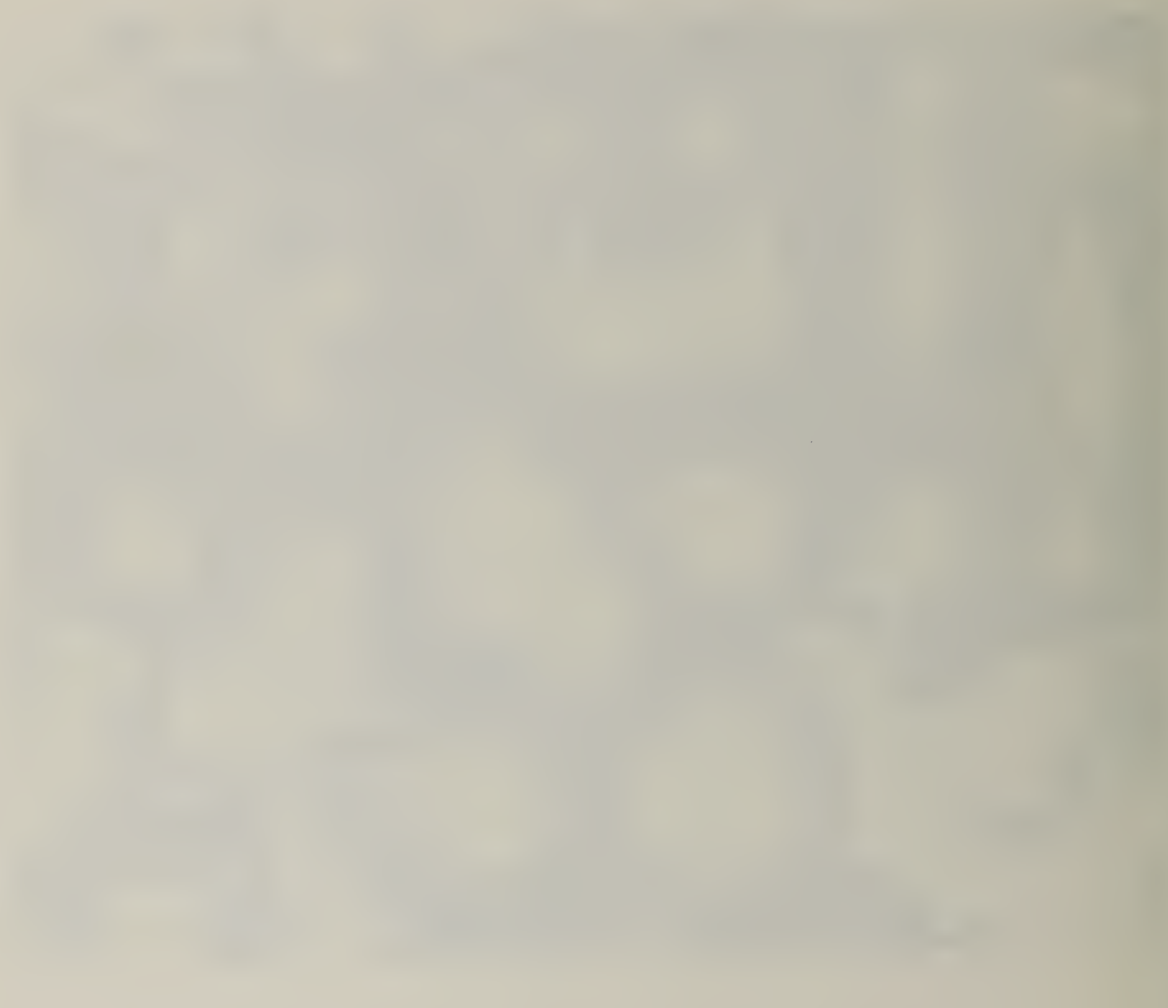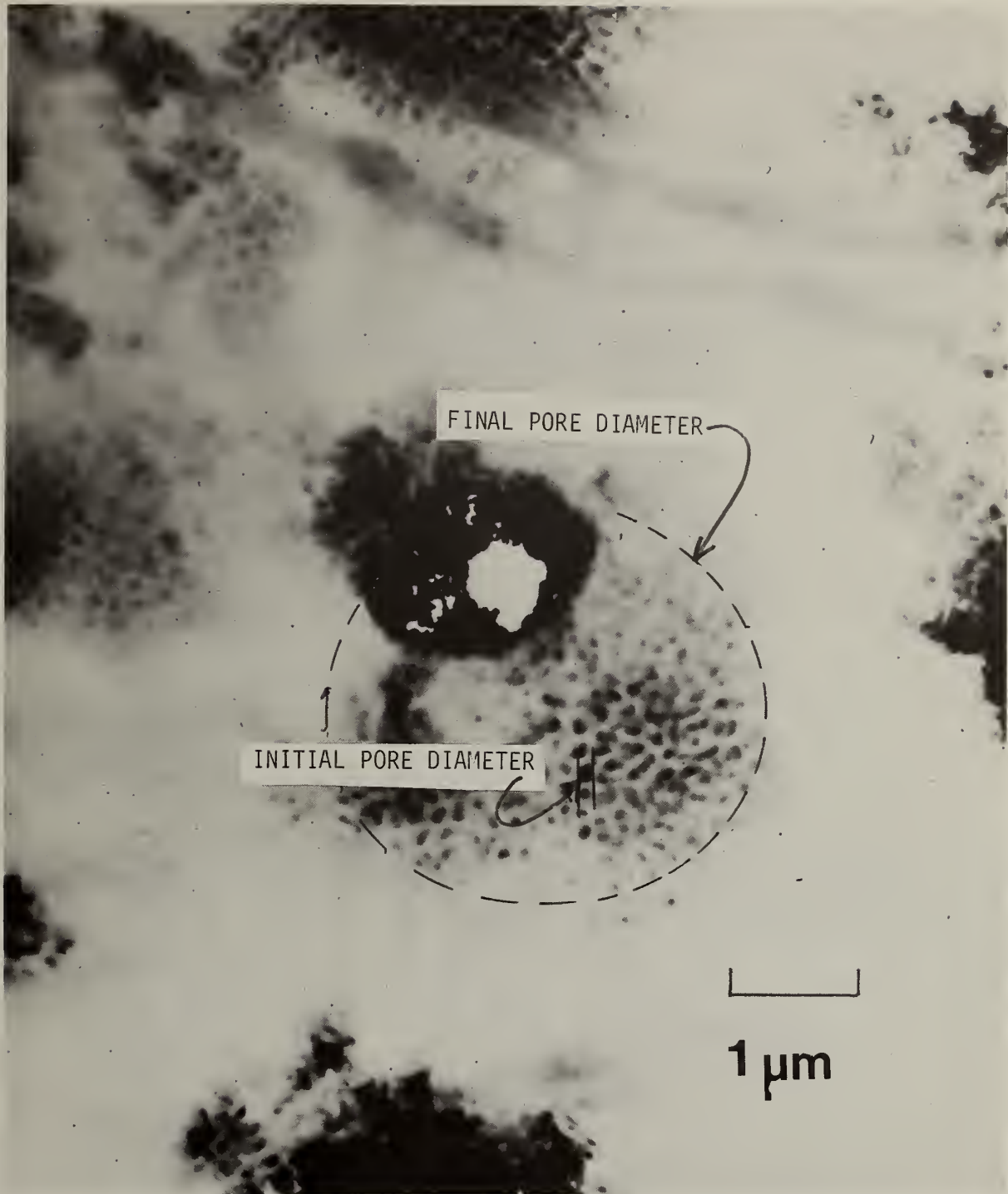
Figure 10. A TEM micrograph showing the transition from the large numbers of small pores formed initially to the large diameter equilibrium pore geometry.
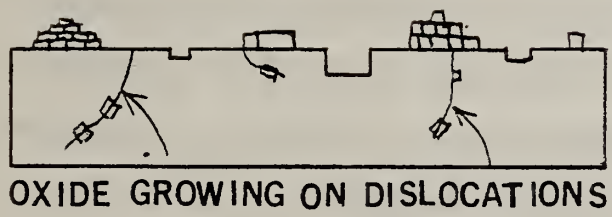
OXIDE GROWING ON DISLOCATIONS

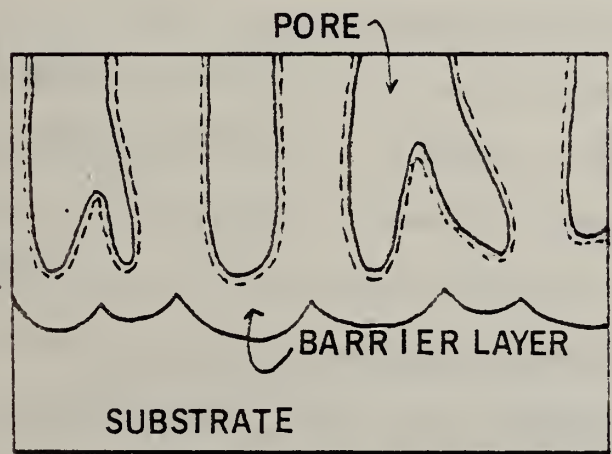Figure 11. A schematic diagram of pore formation on 7000 series alloys: the initial stage.

Figure 12. A schematic diagram of a mature pore structure on 7000 series alloys. (these models are probably not alloy dependent).

At a latter stage of growth the structure of the pore
wall seems to change, as does the location of the place in the
substrate where dissolution occurs. A schematic diagram of a
mature pore (cell) structure is shown in figure 12.

3.3. Electrochemical Measurements:

Three representative alloys 7129-T63, 7146-T6, and 99.99
percent aluminum were investigated to determine if observed
differences in their electrochemical behavior could be correlated
with their subsequent adhesion performance.

3.3.1. Current Density versus Voltage Data:

Current density as a function of anodizing voltage curves
are shown in figure 1. From this data, there appears to be
three distinct regimes of growth, marked accordingly in the
figure. Region one, extending from about 0 to 10 volts,
approximates Ohms Law (V = IR), with a low surface resistance
of from 1 to 2 Ω/cm^2. In region two, this resistance increases
with increasing voltage to a maximum of around 500 Ω/cm^2; in
region three, the resistance becomes small. Clearly, in
region three a dominance of the dissolution process over the
film formation process is apparent. In region one, the surface
is relatively free from large amounts of oxide and, in this
unprotected state, is relatively conductive, so its resistance
is low. Film formation and growth takes place in region two.
As the temperature increases, the rate of film formation
increases, along with the rate of film dissolution. In order
to further examine the initial stages of growth, scanning
voltammagrams of the regions between 0 and 10 volts were made.

3.3.2. Scanning Voltammetry:

Specimens of 1 cm^2 area were prepared for these measurements in the following way. Each was metallurgically polished with the final step being 0.01 μm MgO. This technique yielded reproducible measurements which were comparable to those obtained on electropolished specimens. Simpler grinding techniques yielded spurious data. Results for 99.99 percent aluminum, 7146-T6 and 7021-T63 are shown in Figure 13. Each set of curves corresponds to three successive measurements starting with a freshly polished surface and zero volts, then sweeping the potential to 10 volts (limited by our apparatus), then restarting the sweep. Data from figure 13 is reproduced in Table I.

Table I: Scanning Voltammetry Data.

Alloy	99.99 percent Al	7146-T6	7021-T63
Break pt. on 1st Sweep	3.1 V/SCE	3.5	2.3
Break on all successive sweeps	2 V/SCE	21.9	
Resistance before 1st break in curve	50 Ω/cm^2	37	54
Resistance (steady state)	18 Ω/cm^2	20	18

During the first three volts, the resistance is markedly higher than during the higher voltage regions. This observation implies a lack of significant porous film formation below potentials of three volts/SCE and, probably, pore formation does not start until the first break point, though this
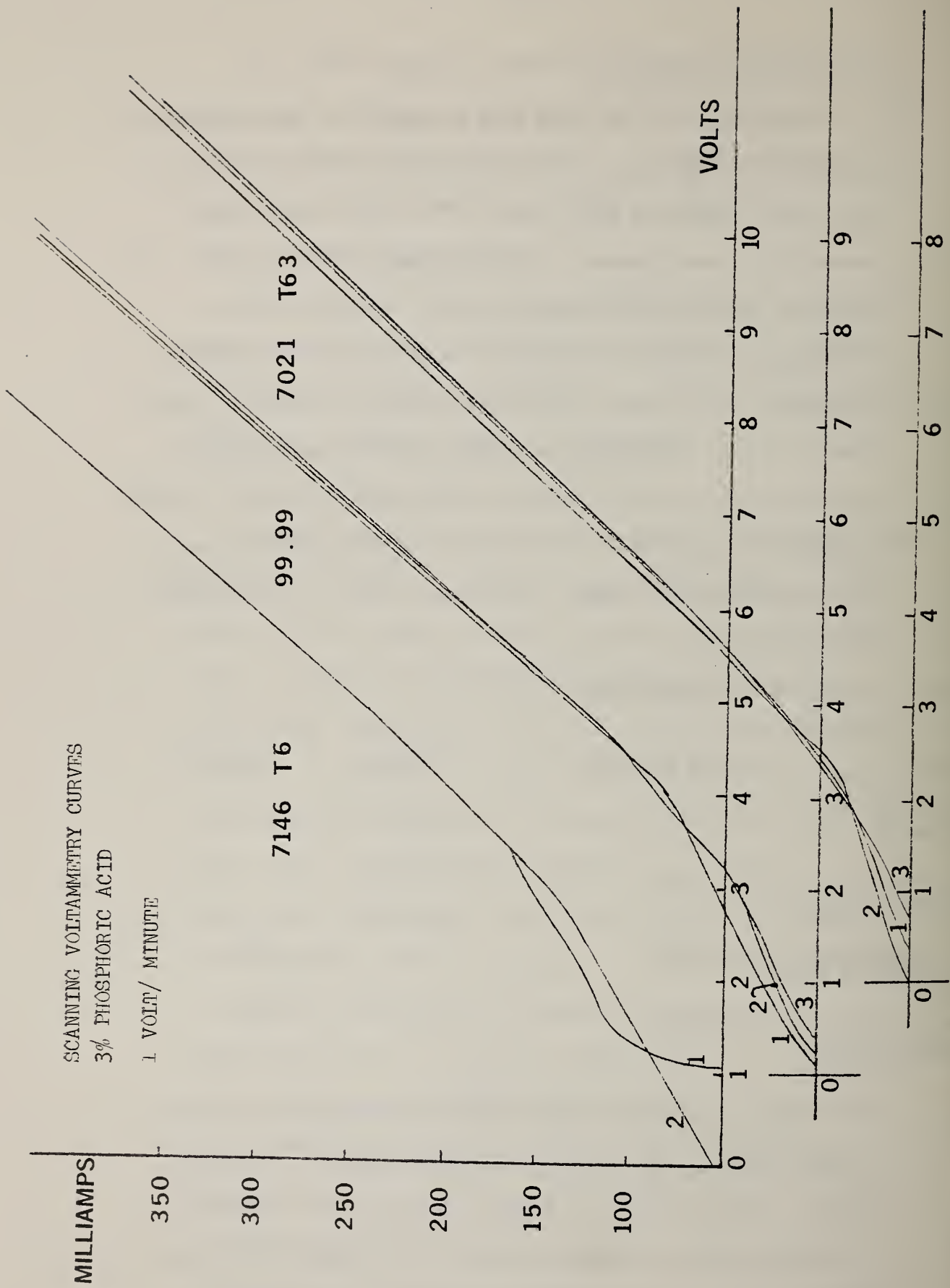
Figure 13. Scanning voltammetry curves for phosphoric acid anodized (a) 7146 T6 (b) 99.99% (c) 7021 T63

has not yet been confirmed. Clearly, there is a reproducible

difference in alloy behavior. It would appear that pore

formation in 7021-T63 and in pure aluminum must have similar

forming rates and, probably, similar morphologies, though this

also has not yet been confirmed. This data was obtained in

three percent phosphoric acid electrolytes at a temperature of

60 °C.

References

1. Ya. I. Alexsandrov, Soviet Electrochemistry, $\underline{15}$, 2(1979) 141
    SEOCAI (2), 137-244 (1979) in English.

2. F. Keller, M. S. Hunter and D. L. Robinson, J. Electrochem. Soc.
    411, (1953).

3. J. P. O'Sullivan and G. P. Wood, Proc. Royal Soc. London A. $\underline{317}$,
    (1970)511.

IV. Immersion Deposition:

Many of the results of the characterization of the immersion
deposition process have been published in previous progress reports
and in appropriate journals and will not be discussed again here.
Some results, however, have not been published. These are the
product of scanning voltammetry and simple dissolution experiments
of zinc films in various acids.

4.1. Scanning Voltammetry:

Specimens of 99.99 percent aluminum were metallographically
polished, with the last step being 0.01 μm MgO. The specimen
surface area was 1 cm^2. The voltammetry experiments were
conducted by switching on the potentiostat just after the
specimen was inserted into the electrolyte. The voltage was
swept at a rate of 1 volt/minute to about -2.1 V. Three or
four specimens were run for each set of parameters to insure
that the data presented below is representative.

In Figure 14a, the curves for the ASTM I electrolyte
(calomel reference electrode) are presented. The H$_2$ peak
appeared only on the reverse sweep. The single dip in the
curve was characteristic of this electrolyte and may be due to
a reduction of the Zn (OH)$^-$ ion to zinc. The voltages shown
with arrows are with respect to the hydrogen electrode.

The results of adding ferric chloride and Rochelle salt
to the electrolyte of Figure 14a are shown in Figure 14b. The
original dip in the curve observed in Figure 14a is still
present, however, with at least three more perturbations
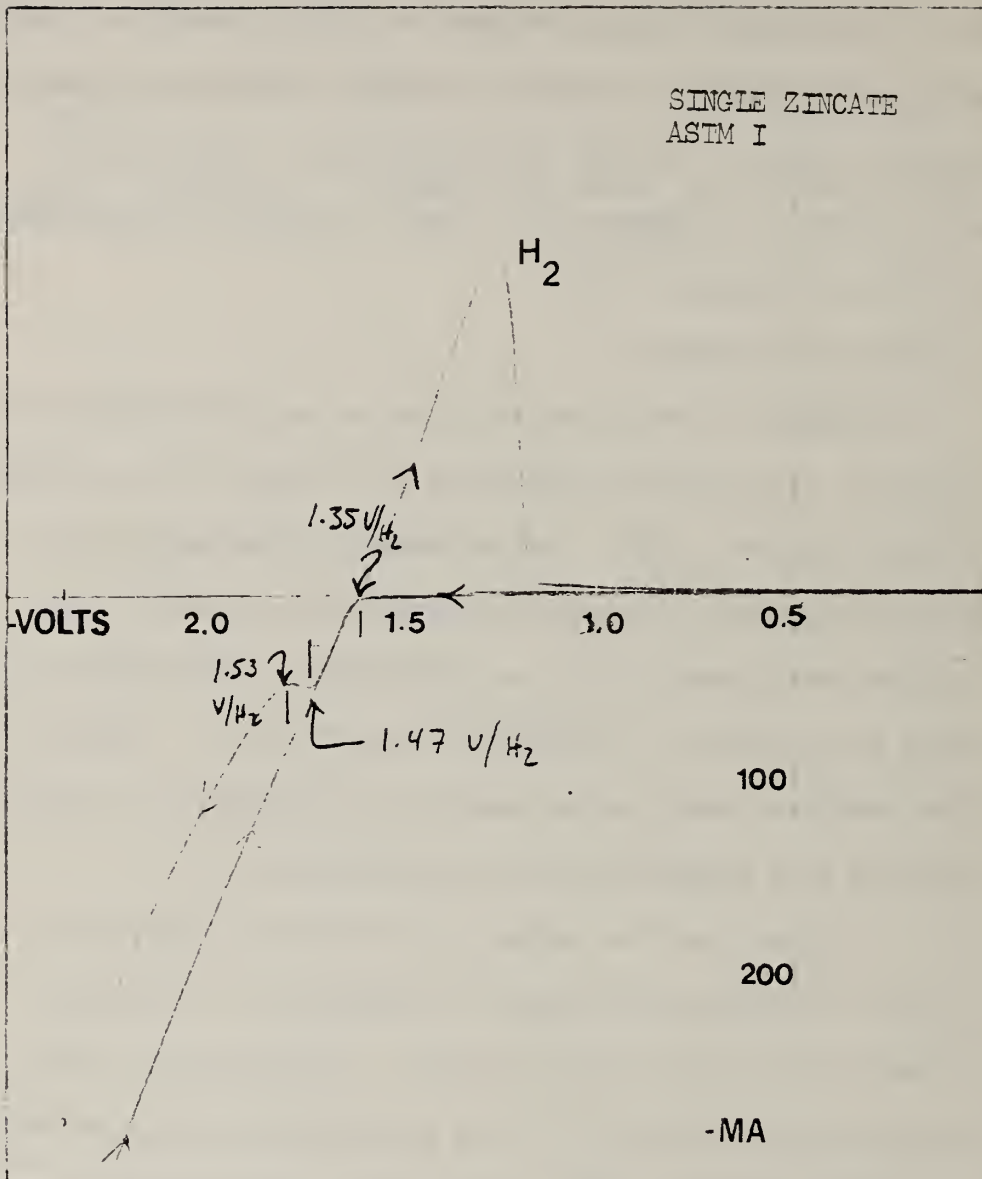apparent. The first, occurring at about 1.44 V(SCE), may be

Figure 14a. Scanning voltammetry curves for the ASTM I zincate electrolyte 99.99% aluminum.
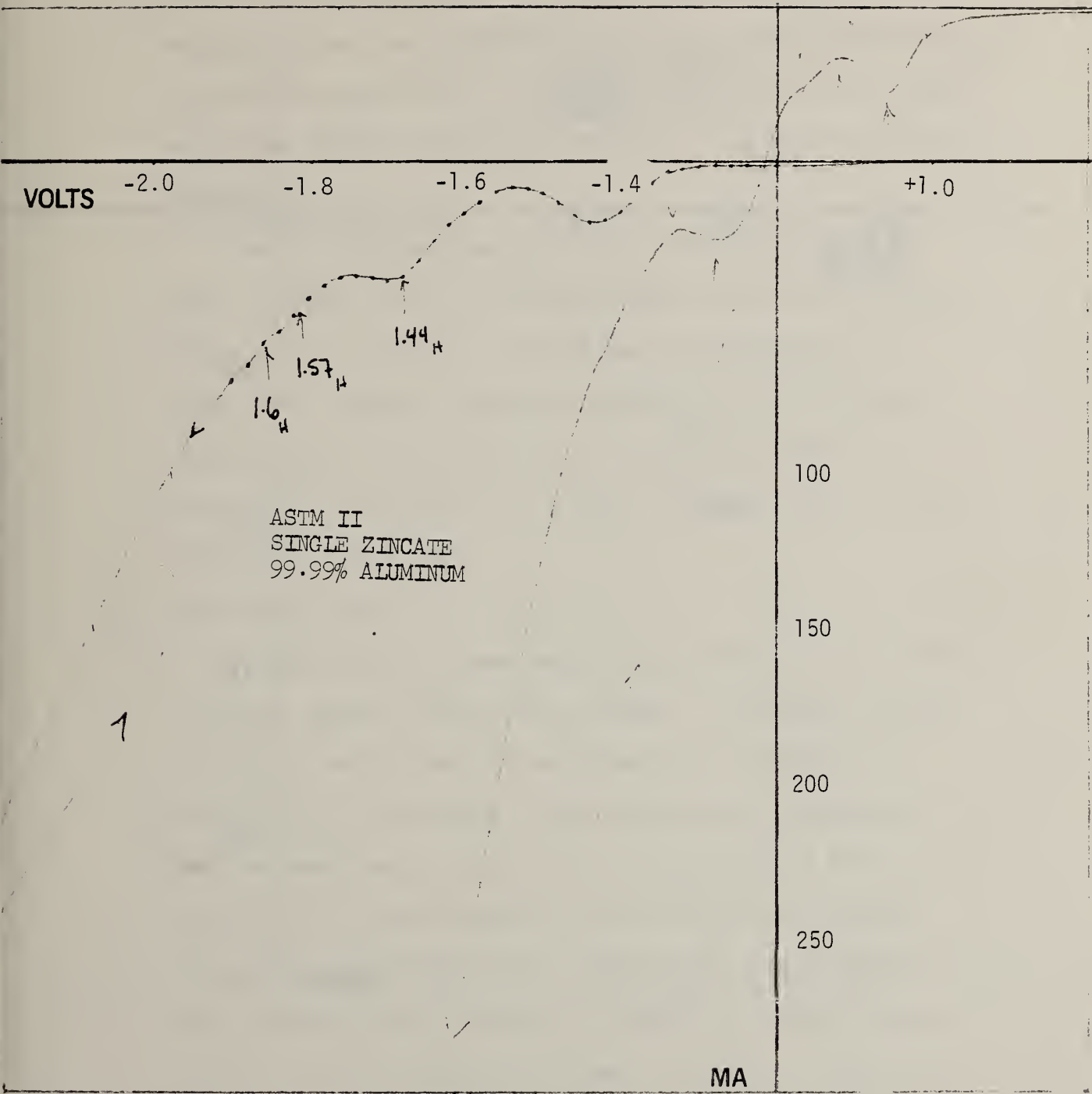
Figure 14b. Scanning voltammetry curves for ASTM II zincate electrolyte. This is the same electrolyte as in 14a with the addition of ferric chloride and Rochelle salt.
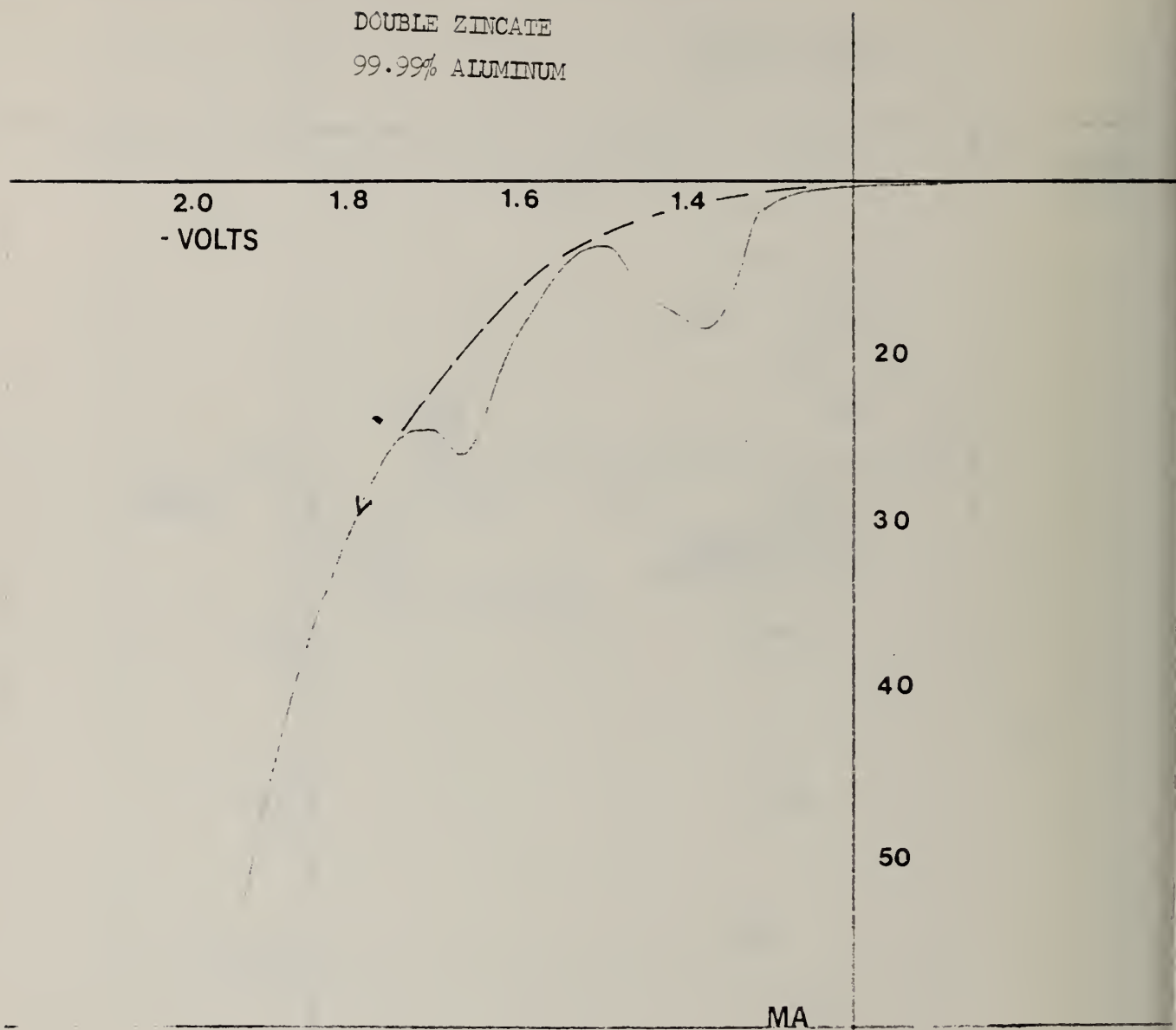
Figure 14c. Scanning voltammetry data for the double zincate procedure with the same electrolyte as in 14b. This date represents the second zinc immersion.

due to a reduction of $Fe(OH)_2^-$ and implies that the iron would be deposited before the zinc. This is consistent with results reported in previous progress reports and by other investigators. The reactions which occur at voltages greater than 1.8 V (SCE) may be due to the reductions of iron-zinc, and Rochelle-zinc, complexes.

The data obtained for the double zincate procedure are shown in Figure 14c, and closely resemble the results from the single zincate procedure from the same electrolyte; i.e. figure 14b. The main difference observed is in the shape of the first peak. Instead of occurring at 1.44 V(SCE), as in figure 14b, it occurs at 1.37 V(SCE). Another peak is clearly observed at 1.44 V(SCE).

4.2. Dissolution Data:

A large number of experiments were conducted in an attempt to further improve the zincate procedure. Specimens of about 12 cm^2 area were buffed and degreased, etch cleaned, and desmutted, as in the normal zincate pretreatment procedure. Most specimens were immersed for one minute in the ASTM III electrolyte at room temperature unless otherwise indicated. The specimens were then placed into various acid solutions and their potential with respect to a calomel or nickel electrode was monitored as a function of time. A typical voltage-time curve is shown in figure 15. In most cases, three or four distinct regions of dissolution are observed. The first part of the curve, region I, is believed to correspond to dissolution

Table I: Summary of Dissolution Data.

| Alloy	Acid	Regions			Remarks
		I sec.	II sec.	III sec.	
6061-T6	5% H_2SO_4, 25 °C	14	13	22	Figure 2 a, ref. Ni.
7129-T63	5% H_2SO_4, 25 °C	3	15	31	Figure 26, ref. calomel Zincate at 40 °C.
1100	1% H_2SO_4	∿12	16	22	Single Zincate, Figure 2 c
1100	1% H_2SO_4	8	8	23	Double Zincate, Figure 2 d
1100	1/2% H_2SO_4	17	23	45	Single Zincate, Figure 2 e
1100	5% H_2SO_4	6	8	12	Figure 2 f
1100	10% H_2SO_4	2	2	4	Figure 2 g
6061-T6	5% H_2SO_4	∿6	6	11	Figure 2 h, ref. Ni.
7146-T6			← 12 →	21	
7146-T6	1/2% H_2SO_4	8	7	36	Figure 2 i
	1/4% H_2SO_4	18	8	>40	
7146-T6	3% H_2SO_4	←——9——→		20	Figure 2 j, 3 min. in zincate
	5% H_2SO_4	←——21——→			
7146-T6	5% H_2SO_4	5	7	26	Double Zincate 2 k
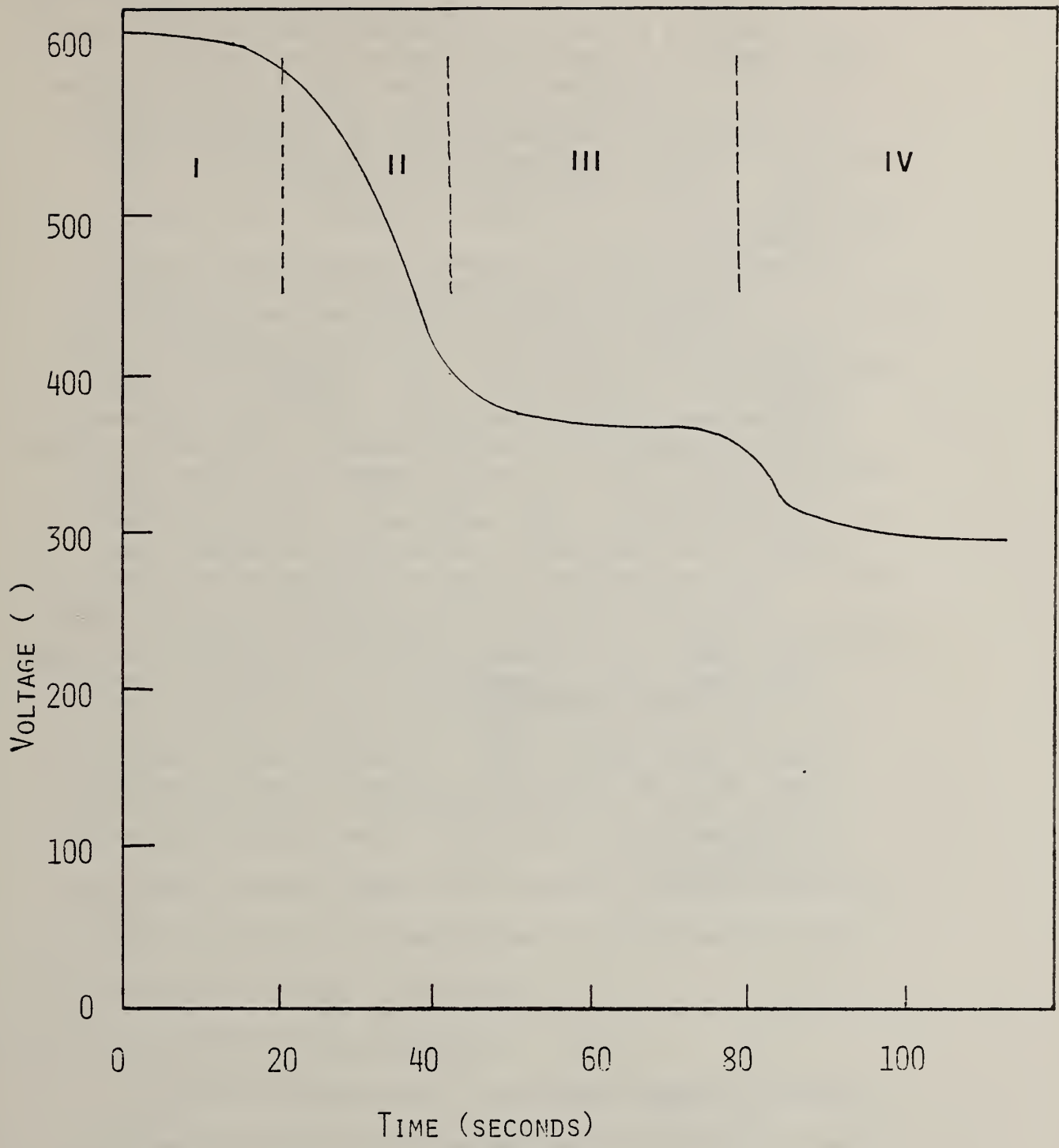
FIGURE 15. A TYPICAL DISSOLUTION CURVE OF ZINCATED ALUMINUM

of the bulk zinc crystallites, and region II to correspond to

a dissolution of the initial zinc layer (see progress reports

III & IV). The rather long plateau, region III, is believed

to correspond to the dissolution of an iron-zinc, or iron

alloy. The data are summarized in Table I.

4.3. Discussion:

The double zincate procedure results in an increase in

the dissolution time of Region III which corresponds to the

dissolution of an iron-zinc alloy. Therefore, the double

zincate procedure is believed to result in enhancement of the

iron alloy coating. This speculation is supported by the

shape of the first peak in the scanning voltammetry data.

Using this dissolution data, specimens were transferred

after Stage I to a sulfamate nickel electrolyte and were found

to form adherent electrodeposits, as was discussed in an

interim report August 1979. This process avoids the use of a

cyanide copper strike but is essentially equivalent to the

ALCOA 661 process.

V. Adhesion Theory

5.1. Adhesion of Metalic Coatings:

Whenever two clean metals are placed in intimate contact, strong adhesive bonding occurs as was shown by Buckley (1). A theory discussing this type of bond was presented by Ferrante and Smith (2). Although the theory of Ferrante and Smith was based on first principles, neither the effect of interfacial dislocations nor the effect of stored strain energy was included in their calculations. Several mechanistic theories that have been published in the literature include the weak boundary layer theory of Bickerman (3) and a Griffith-Irwin type theory presented by Good (4) and others (5-9). An understanding of the forces responsible for bonding are important, not only for electrodeposited coatings, but also for the fields of friction, wear, and fracture. The development of new coatings for materials such as aluminum, in which adhesion is usually a problem, requires an understanding of at least the general mechanism by which metallic coatings adhere to metals. In this paper, current theories of interfacial energy are applied to the calculation of adhesive energy and the specific case of zinc coated aluminum is discussed.

5.1.2. The Effect of Surface Energy:

As has long been known, the adhesion between two metallic surfaces is related to the surface energies of each of the two metals. Consider the total system energy of the metals in contact and compare it to the total system energy when the

metals are separated. The energy difference between the two cases is the adhesive energy per unit area given by,

$$E_{ad} = \gamma_c + \gamma_s - \gamma_i \qquad [1]$$

where γ_c and γ_s are the surface energies of the coating and substrate, respectively, and γ_i is the interfacial energy. Equation [1] does not include either plastic deformation or stored strain energy in the coating or substrate. If two identical metals of different orientations are considered,

then $E_{ad} = \gamma(\text{orientation 1}) + \gamma(\text{orientation 2}) - \gamma_i \qquad [2]$

Therefore, in the case of perfect autoepitaxy ($\gamma_i = 0$), equation [2] becomes

$$E_{ad} = 2\gamma \qquad [3]$$

The relationship given by equation [3] would have to hold no matter where the interface was located. Therefore, equation [3], represents the cohesive energy of the material per unit area. In the case of aluminum, for example, using a bulk value for $\gamma = 840$ ergs/cm^2, the adhesive energy from equation [3] is 1680 ergs/cm^2. This is only an approximate value because the surface energy varies with the orientation and measured values of γ are usually an average of many orientations. If two dissimilar metals are used and γ_i is less than $\Delta\gamma$ where $\gamma_c = \gamma_s + \Delta\gamma$, the adhesive energy would always appear to exceed the cohesive energy of the material with the lower surface energy by the amount $\Delta\gamma$. Therefore, if a normal force were applied to the coated substrate, fracture would occur in

the material with the lower surface energy, and destructive measurements of adhesion, such as peel tests, would be measurements of the cohesive energies of the lower surface energy material and would not be a measurement of true adhesion.

In practice, the interfacial energy γi is not $< \gamma$. Calculations of adhesive energy must take into account the fact that the interfacial energy, γ_i, depends on the crystal structures of the material and the coating, the misfit between these two structures, and the stored elastic strain energy in both the coating and the substrate. The following calculations for adhesive energy make use of the theory of interfacial energy proposed by Jesser and Kuhlman-Wilsdorf (10). Calculations on the zinc-aluminum interfacial shear modulus given in Appendix I are based on data in a paper by Rudman and Averbach (11). In addition, a discussion of the effect of a ·pre-existing crack in the interface on adhesion is presented.

5.1.3. The Effect of Structure:

It is assumed that the potential energy variation experienced by an atom of the coating material moving along the substrate is given by a Peierls-Narbaro function as,

$$V = {}_xV_0 \left[1 - \cos \frac{2\pi x}{{}_xa_s} \right] + {}_yV_0 \left[1 - \cos \frac{2\pi y}{{}_ya_s} \right] + C \qquad [4]$$

where V_0 represents the potential energy amplitude, a_s the lattice constant of the substrate, and C the potential energy/atom of a coating atom when sitting in the bottom of the potential trough. The subscripts x and y refer to the x and y directions. Under these conditions, the adhesive energy is proportional to

an average potential amplitude, $V_o = 1/2(_xV_o + _yV_o)$, for N
atoms, Van der Merve has shown (12),

$$E_{ad} = 2 KNV_o \qquad\qquad [5]$$

where for fcc materials K = 3. The potential V_o is related to
G_o, the shear modules of the interface as was shown by Van der
Merwe as

$$V_o = \frac{G_o a_s}{(2\pi)^2 Nd} \qquad\qquad [6]$$

The subscripts denoting the x and y dependence have been left
out for clarity, and d is the verticle separation between the
coating and the substract. Using this expression for the
average potential amplitude (6) in equation [5], the adhesive
energy per unit area becomes

$$E_{ad} = \frac{K G_o a_s^2}{2\pi^2 d} \qquad . \qquad\qquad [7]$$

Numerical values for the adhesive energies are obtained by
assuming a symmetrical x and y potential distribution and a
close packed configuration with the substrate. The lattice
parameter in the interface is approximated as, proposed by
Jesser and Kuhlman-Wilsdorf (10) by

$$a = \frac{2a_c a_s}{a_c + a_s} , \qquad\qquad [8]$$

and the interfacial shear modulus is calculated with the
assumption of a linear correlation of shear modului with
bonding energy (13). Thus, through the atom spacings of the

coating and substrate, a_c and a_s, the effect of orientation
has been introduced into the calculations of adhesive energy.
For epitaxial deposits of zinc on aluminum (14), the adhesive
energies from equation [7] are given by:

$$Al(111)//Zn(0001), E_{ad} = 1530 \text{ ergs/cm}^2$$

$$Al(011)//Zn(0001), E_{ad} = 1280 \text{ ergs/cm}^2$$

$$Al(100)//Zn(0001), E_{ad} = 930 \text{ ergs/cm}^2$$

Since the cohesive energy of zinc is in the neighborhood of
1480 ergs/cm^2, it is seen that failure will occur within the
interface on (011) and (100) aluminum planes. This calculation
is only a first approximation and more exact caluculations
have to take into account both the existence of interfacial
dislocations and their effect on bonding, and the elastic
strain energy produced as a result of misfit between the
coating and substrate. In the latter case, the dislocation
density should be reduced. Moreover these calculations repre-
sent a minimum adhesive energy. In practice considerable work
would have to be put into the lattice both in the form of
elastic and plastic deformation before planar fracture would
occur.

5.1.4. The Effect of Misfit Dislocations on Bonding Energy:

If a significant misfit between the crystal structure of
the coating and the substrate exixts, a series of interfacial
dislocations will form in such a way as to minimize the resultant
strain energy. The interfacial energy can now be written as

$$\gamma_i = {}_xE_d + {}_yE_d + CN \qquad\qquad [9]$$

where C, represents, as previously discussed, the potential energy of an atom sitting in a potential trough. The number of atoms is given by N and the energy of an array of dislocations by E_d. (Note: $CN = \gamma_s + \gamma_s - 2KNV_o$.) The adhesive energy can now be written as,

$$E_{ad} = 2KNV_o - ({}_xE_d + {}_yE_d). \qquad\qquad [10]$$

The dislocation energy per unit area was shown by Van der Merwe to be given, leaving out the x and y substrates, as,

$$E_d = \frac{G_o}{4\pi^2} \left[1 + \beta - (1 + \beta^2)^{1/2} - \beta \ln \; 2\beta \; (1 + \beta^2)^{1/2} - 2\beta^2 \right] \qquad [11]$$

where $\beta, = \dfrac{2\pi Gb}{P(1 - \nu)(1 + \dfrac{G_c}{G_s})G}$ and is a misfit parameter, P is

the vernier period, $a = \dfrac{a_s a_c}{a_c - a_s}$, and b is the Burgers vector in the interface. By introducing the effect of dislocations into the interface, it is seen that the presence of interfacial dislocation will serve to reduce the adhesive energy over the dislocation free model. The results of calculations for our special case of epitaxial coatings of zinc on aluminum are,

$$Al(111)//Zn(0001): E_{ad} = 1300 \; \text{ergs/cm}^2$$

$$Al(011)//Zn(0001): E_{ad} = 1200 \; \text{ergs/cm}^2$$

$$Al(001)//Zn(0001): E_{ad} = \;\; 840 \; \text{ergs/cm}^2$$

5.1.5. The Effect of Strain Energy on Adhesion:

As a result of misfit between the substrate and the coating, strains will be induced in both the substrate and coating lattices, the density of misfit dislocations, if they exist, will be reduced and the adhesive bonding affected in a complex manner. In the way proposed by Jesser and Kuhlman-Wilsdorf, the new strained lattice parameters at a strain, e, are,

$$a_c' = a_c + a_c e_c \text{ and } a_s' = a_s - a_s e_s , \qquad [12]$$

and the total energy is given by

$$E_{ad} = 2KNV_0 - {}_x E_d + {}_y E_d - E_s . \qquad [13]$$

It was shown by Jesser and Kuhlman-Wilsdorf (10) that the strain energy, E_s, can be expressed as

$$E_s = G_c h_c \cdot \frac{{}_x e_c^2 + {}_y e_c^2 + 2\nu {}_x e_c}{1 - \nu_c} + \frac{{}_x e_s^2 + {}_y e_s^2 + 2\nu {}_x e_s {}_y e_s}{1 - \nu_s} \qquad [14]$$

where ν is Poisson's ratio and h represents coating thickness. The strain, e_c of the coating is given by

$$e_c = \frac{-ba_1 \ln[2\beta' (1 + \beta^2)^{1/2} - 2\beta'^2]}{(1 + \frac{G_1}{G_2}) (a_2 + a_1)(2\pi hc)(1 + \nu)} \qquad [15]$$

For a thick substrate, $e_s = 0$. As a result of strain, however, the dislocation contribution to the interfacial energy will be reduced. A new value for E_{ad} can be calculated from Equation [11] by using equation [12] to calculate new values for the misfit. For zinc coated aluminum the new values of the adhesive energy are:

Al(111)//Zn(0001)., E_{ad} = 1300 ergs/cm^2

Al(110)//Zn(0001), E_{ad} = 1170 ergs/cm^2

Al(001)//Zn(0001), E_{ad} = 800 ergs/cm^2

A comparison between values calculated from the above theory with results of other investigators is shown in Table I.

5.2. The Effect of a Pre-Existing Crack in the Interface on Adhesion:

A pre-existing crack in the interface can result in adhesive failure by reducing the stress necessary to propagate the crack. Such a crack can be a result of poor cleaning, blistering pores, patches of oxide or other causes. The Griffith type model considered in this calculation is shown in figure 16 and consists of a crack of length 2c and unit depth, located in the interface between a substrate of surface energy γ_1, and a coating of surface energy γ_2.

The total surface energy of the crack is then given by

$$E_s = 2c\gamma_c + 2c\gamma_s = 2c(\gamma_c + \gamma_s) \qquad [16]$$

In order to find the stress, σ, at which the crack will just start to propagate, this energy is equated with the
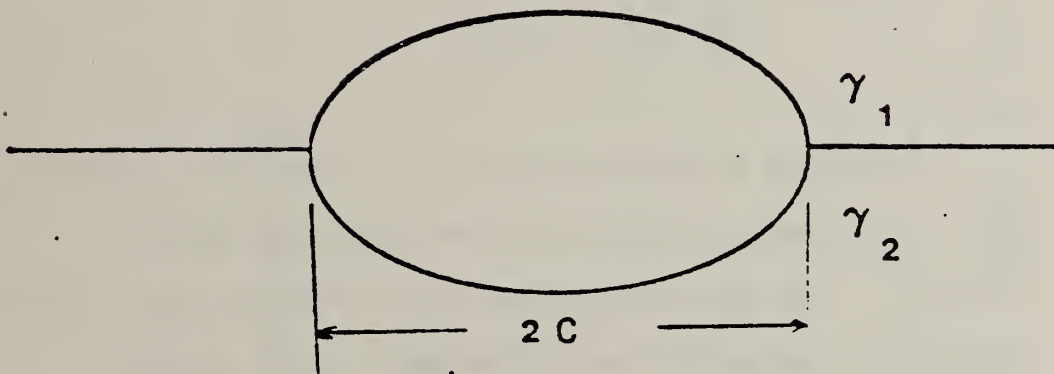
Figure 16. A model for a preexisting crack in the interface. The crack is of unit depth and of length 2C.

stored strain energy as

$$E_{surface} = 2c(\gamma_c + \gamma_s) = E_{strain} = \frac{\sigma^2}{E_c} + \frac{\sigma^2}{E_s} \frac{\pi c^2}{2} \qquad [17]$$

where E represents Young's modulus. Under equilibrium

$$\frac{\partial \left(E_{surface} - E_{strain} \right)}{\partial c} = 0 \qquad [18]$$

so that

$$\sigma_{critical} = \sqrt{\frac{2 \ \gamma_1 + \gamma_2}{\pi c \left(\frac{1}{E_c} + \frac{1}{E_s} \right)}} \qquad [19]$$

In the case of aluminum and zinc, σcritical from equation
[19] is plotted as a function of the crack half length in
figure 17. For crack lengths less than one micron, the stress
necessary to cause delamination exceeds 2 X 10^9 dynes/cm^2
(30,000 psi). For cracks in aluminum only, the stress (Griffith
Criteria) is 1.95 X 10^9 dynes/cm^2 (28,300 psi) and for one
micron cracks in zinc 2.2 X 10^9 dynes/cm^2 (31,900 psi). Note
that once a crack has started, it may run along the interface,
go into the coating or move into the substrate. A more detailed
discussion of crack propagation along an interface was given
by Good (4). In any case, once a crack has started to grow,
the stress necessary to make it continue to grow drops off
very rapidly, so that under conditions of constant stress (and
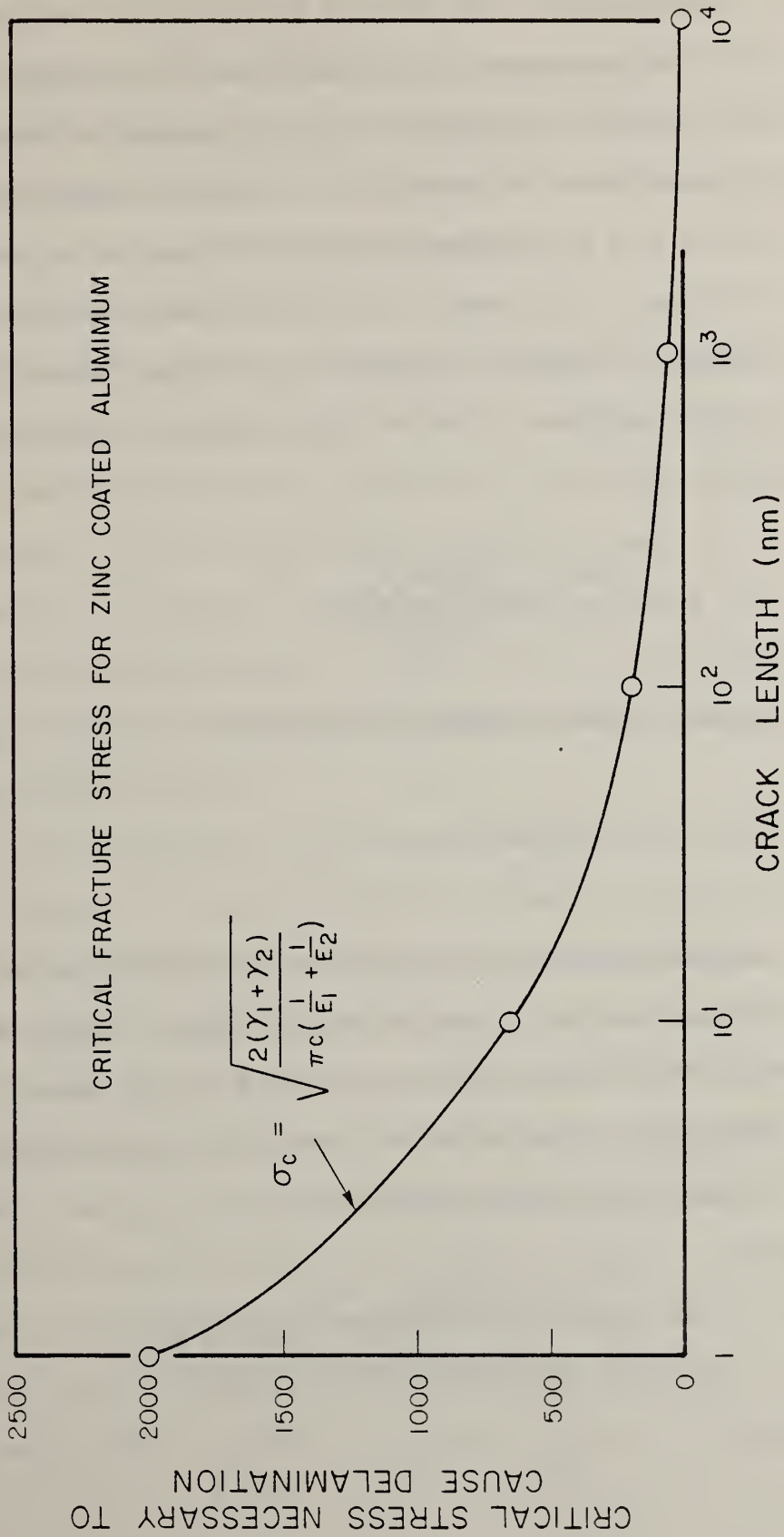
Figure 17. The critical stress required to propagate a crack in the interface for zinc coated aluminum

constant crack radius) the coating will delaminate.

5.3.   Psuedomorphism: the critical radius and the critical thickness:

The phenomenon of pseudomorphism refers to the tendency of a coating to assume the crystal structure of the substrate irrespective of its own crystal structure. The stored strain energy of a pseudomorphic deposit increases with both the thickness of the deposit and with the radius of the pseudomorphic nucleus. Therefore, the deposit is limited in both the radius and the thickness. The critical radius was given by Cabrera (1) to be

$$R_c = \frac{-3b(1 + G_o a_s^2/4G_s a_o^2}{2(1 + G_o/G_s)f} \qquad [1]$$

where f represents the misfit given by

$$f = \frac{a_s - a_o}{a_o} \quad . \qquad [2]$$

The other quantities in equation [1] were defined in the previous section. Using the values for zinc epitaxy on aluminum the critical radius was found to be 4.4 nm or about 20 atom layers thick. The critical thickness for pseudomorphism given by Jesser and Kuhlman-Wilsdorf (2) as

$$Hc = \frac{-G_2 b^2 \ln \dfrac{-4\pi G_1 G_2 (a_2 - a_1)}{(G_1 + G_2)G(1 - \partial)(a_1 + a_2)}}{2\pi a_2 f(1 + z\partial)(G_1 + G_2)}$$

where for the zinc-aluminum system on the (111) aluminum plane the critical thickness was found to be 0.2 nm or about 1 (at most) monolayer. These calculations seem to preclude this phenomenon of being of practical importance because crystals of zinc immersion deposited on aluminum are commonly observed as being of larger thickness and radius.

Discussion and Conclusions:

Both the existence of interfacial dislocations and the stored elastic strain energy contribute in a significant way to the adhesion of metallic coatings on crystalline aluminum substrates. For non-crystalline substrates, aluminum or otherwise, the adhesive energy for metallic coatings (both crystalline and amorphous), is higher than for the comparable crystalline material because of the higher surface energy of the amorphous material.

Calculations have been presented only for the case of zinc coatings on aluminum substrates; however, a basis exists for future calculations of the relative adhesion between nickel, iron, copper, tin and various alloy coatings to aluminum, and results for these materials will be reported in the future. It was shown above that for zinc and aluminum the greatest adhesive energy occurs when coatings are deposited on (111) aluminum compared to the other principle planes. In general however, the adhesive energy will vary with the surface energy so that for fcc materials the adhesion will decrease in the following order: $E_{ad}(110) > E_{ad}(100) > E_{ad}(111)$. Moreover

from equation [7], it is predicted that the higher index planes (greater surface energy planes) would exhibit greater adhesion than the principle planes. Since extruded parts can be made in thicker cross section than the comparable rolled sheet, the incentive of improved adhesion may make a change to extrusions desirable.

In Table I a comparison between the adhesive energy determined by a number of different techniques is presented. The definition of adhesive energy used by Ferrante and Smith differs from the definition used in this paper by exactly a factor of two. When allowance is made even for this, the adhesive energies are still below these calculations by a factor of about 20 percent. It should be noted that Ferrante and Smith did not take into account the lattice mismatch between the zinc and the aluminum, nor did they take into account the stored strain energy. These factors would have reduced their values even further.

The surface energy of alloys is in general greater than the surface energy of pure aluminum and is proportional to the ultimate tensile strength. It would then seem that adhesion on alloys would be proportionally greater than on pure aluminum. This does not seem to be the case, however. One, therefore, draws the conclusion that this discrepancy is the result of either incomplete coverage of the surface, due to incomplete oxide removal, or defects in the zinc layer resulting in the existence of a crack. One cause of this, would be imcomplete coverage over alloying constituents.

Table 1. Adhesive Energy for Various Coating – Substrate Combinations (ergs/cm^2)

Substrate	Coating	$\gamma_c + \gamma_s$	Ferrante and Smith[2]	E_{ad}	$-E_d$	$-E_s$	E_{total}	Experiment: Rabinowicz[15]
Al	Al	1680	405	934	-	-	934	900
(100)	Zn	1580	360	928	87	30	811	900
(110)				1283	85	30	1168	
(111)				1531	200	30	1301	
Al	Mg	1390	320	813				
Al	Cu	1940		1175				
Al	Ni	2590		1517				
Zn	Zn	1480	320	1332				5700
Zn	Mg	1290	285					
Mg	Mg	1100	255	690				
Ni	Ni	3500		2040				1750
Ni (100)	Cu	2850		1723	164	0	1559	
(110)				2100	98	0	2000	
(111)				2226	114	0	2112	
Cu	Cu	2200	320	1070				2333

LIST OF FIGURES

NBS-114A (REV. 9-78)

U.S. DEPT. OF COMM. BIBLIOGRAPHIC DATA SHEET	1. PUBLICATION OR REPORT NO. NBSIR 80-2142	2. Gov't. Accession No. .	3. Recipient's Accession No.

4. TITLE AND SUBTITLE Anodizing and Immersion Processes	5. Publication Date November 1980
	6. Performing Organization Code

7. AUTHOR(S) Dr. David S. Lashmore	8. Performing Organ. Report No.

9. PERFORMING ORGANIZATION NAME AND ADDRESS NATIONAL BUREAU OF STANDARDS DEPARTMENT OF COMMERCE WASHINGTON, DC 20234	10. Project/Task/Work Unit No.
	11. Contract/Grant No.

12. SPONSORING ORGANIZATION NAME AND COMPLETE ADDRESS (Street, City, State, ZIP) Aluminum Association, Inc. 818 Connecticut Avenue, N.W. Washington, DC 20006	13. Type of Report & Period Covered
	14. Sponsoring Agency Code

15. SUPPLEMENTARY NOTES

☐ Document describes a computer program; SF-185, FIPS Software Summary, is attached.

16. ABSTRACT (A 200-word or less factual summary of most significant information. If document includes a significant bibliography or literature survey, mention it here.)

This report summarizes results on the "Plating on Aluminum" project, which was sponsored by the Aluminum Association. The program includes both anodizing and immersion pretreatments as well as a discussion of adhesion. In addition to the summary of results, some details of the last seven months of the project are presented including: (a) the morphology of the initial stages of anodic film formation; (b) the morphology of the interface of nickel coated anodized aluminum; and (c) a discussion of adhesion.

17. KEY WORDS (six to twelve entries; alphabetical order; capitalize only the first letter of the first key word unless a proper name; separated by semicolons)

Adhesion; anodizing; coatings; electrodeposition; immersion deposition; plating; plating on anodized aluminum

18. AVAILABILITY [x] Unlimited	19. SECURITY CLASS (THIS REPORT)	21. NO. OF PRINTED PAGES
☐ For Official Distribution. Do Not Release to NTIS	UNCLASSIFIED	63
☐ Order From Sup. of Doc., U.S. Government Printing Office, Washington, DC 20402, SD Stock No. SN003-003-	20. SECURITY CLASS (THIS PAGE)	22. Price
[X] Order From National Technical Information Service (NTIS), Springfield, VA. 22161	UNCLASSIFIED	$7.00

USCOMM-DC